Journal Article

A computational study of the influence of surface roughness on material strength

McMillan, A, Jones, R, Peng, D, Chechkin, G.A.

A computational study of the influence of surface roughness on material strength

Alison McMillan[1], Rhys Jones[2], Daren Peng[2], Gregory A Chechkin[3]

[1] School of Applied Sciences, Computing and Engineering, Wrexham Glyndwr University, Mold Road, Wrexham, LL11 2AW, UK.
[2] Department of Mechanical and Aerospace Engineering, Monash University, Clayton, VIC 3800, Australia.
[3] Department of Differential Equations, Faculty of Mechanics and Mathematics, M.V. Lomonosov Moscow State University, Moscow, 119991, Russian Federation.

alison.mcmillan@physics.org

Abstract. In machine component stress analysis, it usually assumed that the geometry specified in CAD provides a fair representation of the geometry of the real component. While in particular circumstances, tolerance information, such as minimum thickness of a highly stressed region, might be taken into consideration, there is no standard practice for the representation of surface quality. It is known that surface roughness significantly influences fatigue life, but for this to be useful in the context of life prediction, there is a need to examine the nature of surface roughness and determine how best to characterise it. Non-smooth geometry can be represented in mathematics by fractals or other methods, but for a representation to have a practical value for a manufactured component, it is necessary to accept that there is a lower limit to surface profile measurement resolution. Resolution and mesh refinement also play a part in any computational analysis undertaken to assess surface profile effects: in the analyses presented, a nominal axi-symmetric geometry has been taken, with a finite non-smooth region on the boundary. Various surface roughness representations are modelled, and the significance of the characterized surface roughness type is investigated. It is shown that the applied load gives rise to a nominally uni-axial stress state of 90% of the yield, although surface roughness features have the effect of modifying the load path, and give rise to localized regions of plasticity near to the surface. The material of the test model is assumed to be elasto-plastic, and the development and evolution of plastic zones formed within the geometry are shown for multiple load cycles.

Keywords: FEA; Surface roughness; Residual stress; Fatigue strength; Fractal; Geometry

1. Introduction

In machine component stress analysis, such as performed high duty engineering components used in the aerospace or rail industry, the geometry of the component is typically provided electronically in the form of a CAD file. The information included generally indicates the nominal geometry and tolerances. If there is any definition for surface finish, it is generally descriptive rather than prescriptive, *e.g.* a "mirror finish", or it is implied by a manufacturing instruction, *e.g.* "milling", "lapping" or "interference fit". Depending on the component, R_a values are also used, where R_a is the "Arithmetical Mean Roughness" [1, 2]:

$$R_a = \frac{1}{n} \sum_{i=1}^{n} |y_i| \qquad [1]$$

where y_i is the vertical distance from the ith measured surface point to the mean line of the surface.

Often there are features, such as fillet radii, edge smoothing, as well as features such as metrology markers and component identification number markings, which are ignored for the purposes of stress analysis. Furthermore, in complex geometrical constructions, it is sometimes the case that there are surfaces and vertices that do not quite meet, which might incur some geometry repair judgement to be made by the stress engineer. It is therefore clear that there can be a subtle difference between the geometry of the actual component, the as-drawn geometry, and that used for the stress analysis.

In usual practice, the stress engineer will take the nominal geometry, and use judgement to simplify the geometry; sometimes removing features that are unlikely to experience high stresses or influence the stress state in the regions of more interest. On examination of the stress analysis results, he or she might refine the model, re-instate such details, adopt a higher resolution mesh, or possibly even modify geometry for worst tolerance: each of these actions might be required depending on how close the stress values are to the limits of acceptability for that particular component. It is quite likely that there would be some feedback to the component designer, indicating beneficial geometry modifications: these days, this might be streamlined through the use of a design optimization design-stress workflow.

If the duty of the component includes cyclic loading, the stress engineer will also consider fatigue life. Generally, this focusses on the loading regimes and the corresponding numbers of cycles. Although it is known and understood that surface finish influences fatigue life, this is often compartmentalized as a materials test issue: surface finish is specified for fatigue test coupons. Outside of the aerospace industry it is rare that a specific component surface finish is specified in order to meet a particular fatigue life requirement. Generally fatigue life prediction is considered a crude assessment, so that it is necessary to validate the life of a component by testing to substantively higher numbers of cycles than the life to be certified. The US Joint Services Structural Guidelines JSSG2006 requires that to certify an airframe the structure withstand two lifetimes of testing without failure [3]; for gas turbine engine critical parts, the requirement involves statistical analysis to of both the fatigue test data and component tolerance [4].

Where both tolerance and surface roughness are concerned, the question as to the significance of exact geometry is generally answered by invoking the Saint Venant principle [5], which is explained by Love [6] as "…the difference between the effects of two different but statically equivalent loads becomes very small at sufficiently large distances from load". Since small changes in component geometry will influence the load path and these the stress distribution within the component, the Saint Venant principle is also applied to small changes in geometry. This question has been explored by a number of authors [7–9] in the context of the justification of geometric simplification in initial stress analyses and subsequent redesign for enhanced performance. On closer consideration, it should be remembered that the Saint Venant principle applies to the gross stress distribution through the volume of the component: it clearly cannot apply to the regions of the component in close proximity to any geometric variation. In other words, the stress state in a region at some reasonable distance from a geometric variation will not be significantly influenced by it; however, the stress state in the

neighbourhood of the geometric variation will be substantively different to that predicted for the nominal geometry. In some cases, the stress-raiser effects might lead to localized plasticity [10], and the evolution of the plastic zone over repeated load cycles should cast light on the understanding of fatigue where the nominal component stress state might be well below yield.

2. Surface Roughness

2.1. Implication of manufacturing process on surface geometry
Different component manufacturing processes have a different impact on the surface finish. A thorough consideration of this would include both additive [11] and subtractive manufacturing processes, but for high performance components, even those made to near net shape, the finishing process for the bulk of the component surface is usually subtractive. Subtractive processes include machining techniques such as turning, drilling and milling, which result in a surface profile which has fairly regular spatial features with a length scale of between fractions to tens of micrometres [12]. The highest level of smoothness achievable by conventional mechanical machining is that of polishing, which, under very special process control, can reduce the length scale to the order of tens of nanometres [13].

A further aspect for consideration is post-manufacture surface treatments which are designed to introduce residual compressive stresses near the surface. The purpose is to suppress the opening of cracks near the surface, thereby enabling the component to perform at a higher level of duty than would otherwise be the case. Such techniques include shot peening, plasma-nitriding and laser shock peening, among others. The question is this: if such treatments introduce surface texture modifications, how much does this detract from the benefit provided by the compressive residual stresses, particularly for components subject to cyclic loading [14]?

2.2. Representation of surface roughness
Although "surface roughness" is a concept known by everyone, when used in the context of manufacturing, it is a descriptive concept. What is required is a means to characterize it in a way that is representative of the essential aspects of reality, and which ideally defines a recipe for constructing sufficiently similar artificial geometries for the purpose of modelling. In this context Mandelbrot [15] established that surface roughness can be uniquely characterized by the fractal box dimension D. Interestingly, fractal concepts are now used to characterize crack growth [16–18] and form the basis for assessing crack growth in RAAF operational aircraft [19].

Surface roughness can have an impact on numerous other engineering aspects in addition to strength and fatigue life. Further consider that the method for achieving a particular surface might be through means other than conventional machining processes. As such, there would be a requirement for a different method of surface characterization, and this also has implications for property model standardization, whereby the classification of surface roughness becomes another property to be incorporated within ISO standards such as STEP and the recently proposed ISO 25178 [2, 20].

In the case studies to be presented here, the primary need was to simplify these geometric representation problems, and to present results that would be sufficiently indicative of reality as to prompt further more detailed study. Representation of complex 3D geometry [21] is possible but problematic. In this study an axi-symmetric geometry was chosen, on the basis that this could be considered representative of a component made by a turning process. This enables a simpler geometry definition and aids in presenting the results.

The computational analysis was performed using finite element analysis, and as far as possible to ensure a regular element distribution by using to "pixel" grid of elements in the surface roughness region. This approach is limited at the lower bound, by both the limit to which the geometric profile can be represented, and by the computational approximations of the analysis.

In practical terms, any physically direct measurement of the surface profile of a component will yield tabulated results of depth or height from nominal at a regular grid interval. Such data lends itself

naturally to a grid representation. Lateral shapes, such as overhangs or tapered valleys, would not be captured directly, but should be considered.


| (a) | (b) | (c) |
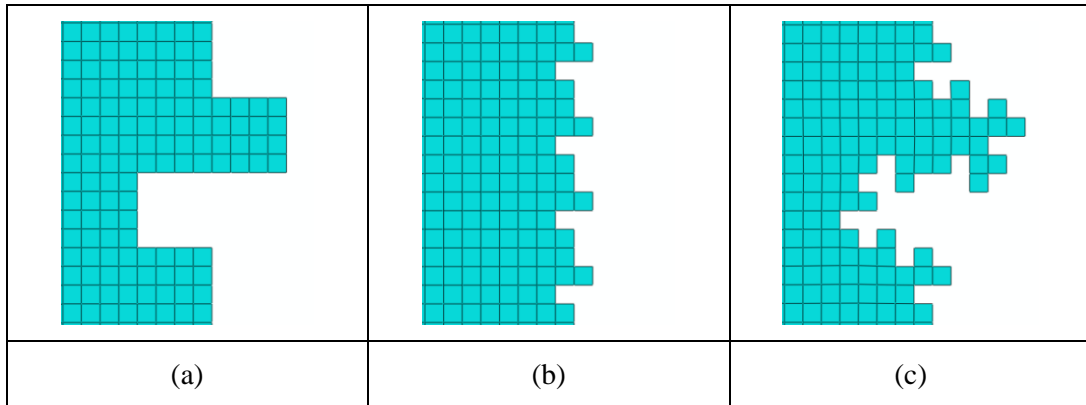
Figure 1. Three representations of surface roughness.

2.3. Fractal shapes applied to finite element geometry

As previously mentioned, the representation of surface roughness as a fractal was first proposed by Mandelbrot [15]. This approach has the potential to provide the systematic recipe for surface roughness profile creation.

The fractal family adopted for this study is known as the "Minkowski sausage" or "Koch curve (type 2)". It was chosen because it can be easily constructed using a regular grid, and this meets the need for a regular finite element mesh. The basic form is shown in Figure 1(a), replicated and scales in Figure 1(b) and then the form is re-applied to the original, as shown in Figure 1(c).

In a fractal representation of the boundary, the same form is re-applied, in descending scale, *ad infinitum*. The Hausdorff dimension provides a measure of the ratio of the surface length to enclosed area. For the Minkowski sausage, the Hausdorff dimension is 1.5. In computational analysis, only a finite number of levels can be modelled, although the real limit to the minimum feature scale is potentially that of the atomic scale of material.
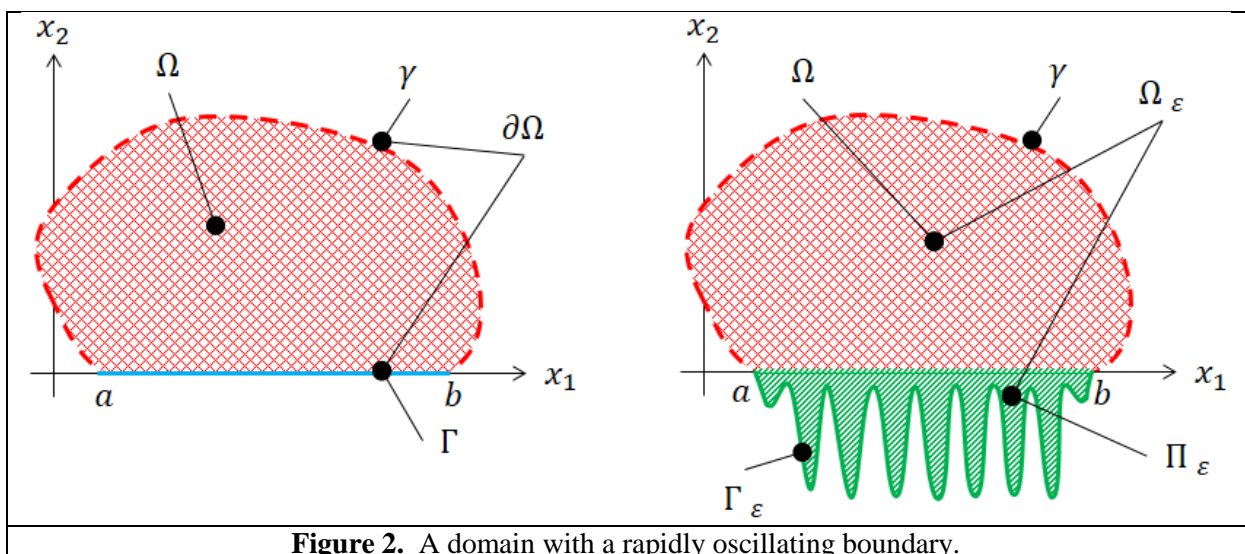
Figure 2. A domain with a rapidly oscillating boundary.

2.4. Mathematical bounds on the effects of surface roughness using the homogenization procedure

The homogenization procedure [22–27] provides a method for substituting a problem involving a material domain with a rough boundary, by a corresponding domain with a smooth boundary, together with modified boundary conditions. By defining bounds to the surface roughness profile, it is possible to create correspondingly bounded correction terms to the solution to the differential equation, in this case, the stress-strain.

Let us consider a model plane in which a smooth domain Ω is situated in the upper half space of the $\mathbb{R}^2$ plane, see Figure 2. A part of its boundary coincides with the segment Γ, which is (a,b) on the abscissa axis. This segment Γ is the smooth replacement for the rough boundary, Γ_ε. The region of surface roughness is the domain enclosed above by segment Γ and below by the rough boundary, Γ_ε is denoted by Π_ε.

Π_ε is expressed mathematically as the domain $\{x \in \mathbb{R}^2 : x_1 \in [a,b], 0 \geq x_2 > \varepsilon F(x_1, x_1/\varepsilon)\}$, where $F(x_1, \xi_1)$ is a smooth function for which $F(x_1, \xi_1) \leq 0$ if $x_1 \in [a,b]$, and $F(a, \xi_1) = F(b, \xi_1) = 0$. We also demand that $F(x_1, \xi_1)$ is "1-periodic" in ξ_1 (periodic in ξ_1 with period 1); thus F is a locally periodic, smooth function, which vanishes at the end points of the segment Γ, at $(a, 0)$ and $(b, 0)$, on the plane of $\mathbb{R}^2$. Additionally, the lower, rough boundary, Γ_ε, of the set Π_ε is defined as rapidly oscillating locally periodic. In other words, the function F defines the rough boundary, Γ_ε between the end points a and b. The behaviour of this function is illustrated in schematic form, in Figure 2: it intersects with the smooth boundary at the end points, and it always lies outside the smooth boundary between those end points.

The complete domain, Ω_ε, including the smooth domain and the region of surface roughness, is defined as $\Omega \cup \Pi_\varepsilon$. It is useful to define the common boundary of both Ω and Ω_ε, that is, the part of the boundary not including the segment Γ or Γ_ε, as γ. This is written mathematically as $\gamma = \partial\Omega \setminus \Gamma$.

For the purposes of the example here, we present the model problem in Ω_ε for the Laplacian operator, Δ, although in principle any partial differential operator could be applied, including the mathematical system of elasticity, expressing Hooke's law in terms of displacements and (strains) stresses.

The problem can be expressed as follows:

$$\begin{cases} -\Delta u_\varepsilon(x) = f(x), & x \in \Omega_\varepsilon, \\ u_\varepsilon(x) = 0 & x \in \gamma, \\ \dfrac{\partial u_\varepsilon}{\partial v_\varepsilon} + p\left(x_1, \dfrac{x_1}{\varepsilon}\right) u_\varepsilon = q\left(x_1, \dfrac{x_1}{\varepsilon}\right), & x \in \Gamma_\varepsilon, \end{cases} \qquad [2]$$

where $p(x_1, \xi_1)$ and $q(x_1, \xi_1)$ are sufficiently smooth non-negative 1-periodic functions in ξ_1, and v_ε is the outer unit normal to the boundary Γ_ε.

This can be compared with the following "limit" (homogenized) problem with an "effective" boundary condition:

$$\begin{cases} -\Delta u_0(x) = f(x), & x \in \Omega, \\ u_0(x) = 0 & x \in \gamma, \\ -\dfrac{\partial u_0}{\partial x_2} + P(x_1) u_0 = Q(x_1), & x \in \Gamma, \end{cases} \qquad [3]$$

where

$$P(x_1) = \int_0^1 p(x_1, \xi_1) \sqrt{1 + \left(\frac{\partial F}{\partial \xi_1}\right)^2} \, d\xi_1, \quad Q(x_1) = \int_0^1 q(x_1, \xi_1) \sqrt{1 + \left(\frac{\partial F}{\partial \xi_1}\right)^2} \, d\xi_1. \qquad [4]$$

Here it can be seen that the problem defined over the domain with the rough boundary can be re-written for a domain with a smooth boundary by modifying the boundary conditions that are applied to the replaced boundary. Note that because the function u_0 is sufficiently smooth, it can be evaluated for locations within the region of surface roughness Π_ε. This makes approximation of the solution possible [28], making use of the following theorem:

Theorem 0.1 *The estimates*

$$\int_{\Omega_\varepsilon} (u_\varepsilon - u_0)^2 \, dx \leq K\varepsilon^2, \quad \int_{\Omega_\varepsilon} |\nabla u_\varepsilon - \nabla u_0|^2 \, dx \leq K\varepsilon \qquad [5]$$

hold true, where K is independent of ε. This theorem can be reformulated for the model problem of elasticity, with the estimates written in terms of displacements and stresses.

The case of very rapidly oscillating boundaries is treated in [29]. In very rough boundaries, the boundary Γ_ε can be defined by $x_2 = \varepsilon F(x_1, x_1/\varepsilon^\alpha)$, with $\alpha > 1$. For the treatment of randomly defined surface roughness, see [30–33].

There are a number of difficulties in using Equation [5] in a practical determination of the change in the local stress or strain arising from a rough surface. The biggest difficulty is that the expression involves an integration over the complete domain of the component, and therefore provides no easy method to assess local effects distributed over a small domain within the component. A second difficulty is that although the bound is quantified by the factor K there is no practical method for its calculation. The third difficulty is that the theorem is stated for linear elasticity only.

There is an additional observation that the rough surface is defined as being outside the nominal surface – it is defined differently to R_a (Arithmetical Mean Roughness). In the context of comparison of surface roughness metrology measures, one might consider alternatives to R_a, such that the definition is consistent with the definition of F. In doing so, it becomes apparent that the choice of the measure is practically equivalent to the choice of Γ_ε and drives the tolerance of the predicted result.

3. Computational test case: an axisymmetric specimen

3.1. Geometry and material considerations

For the purposes of this investigation, a very simplistic nominal geometry has been chosen, based on an axi-symmetric axial test specimen. Such a specimen has a narrow gauge section, wherein the state of stress is considered to be uniformly distributed and uniaxial. In the manufacture of test specimens close attention is paid to the surface finish in the gauge section, as surface flaws can influence the test result, for example [34] specifies that the specimen be polished prior to testing. Other studies of the effect of surface finish on mechanical properties include [35, 36]. Since, in general, this level of surface modification is not carried out on in-service components; one focus of the present paper is to quantify the effect of this surface polishing process.

This computational study assumes the presence of flaws that extend circumferentially around the specimen. Where such surface flaws arise from a turning type operation with a low feed-rate, then this assumption is reasonable. Flaws of a more localized nature, or obvious helix form would require a different analysis model.
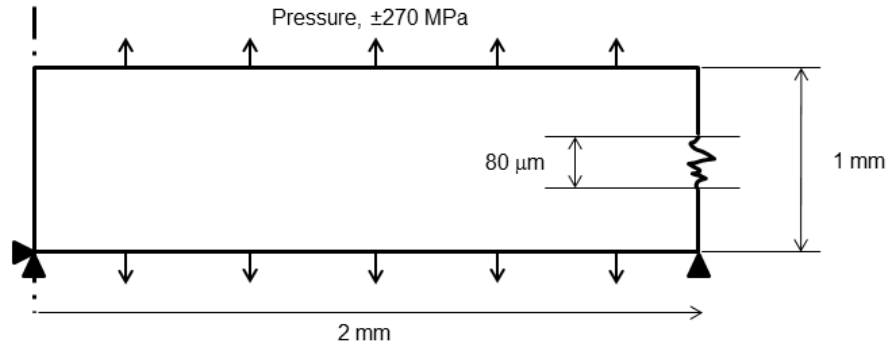
Figure 3. Axi-symmetric test-piece geometry.

The modelled geometry is shown schematically (not to scale) in Figure 3. The specimen has been truncated, to include only the gauge section, and within this, surface roughness is confined to a narrow central band. This ensures that with surface pressure loading the stress distribution is sufficiently uniform above and below the central band. Dimensions are given in Table 1. These dimensions were chosen to be representative of a laboratory scale test specimen, where realistic sized surface roughness features would remain very small compared with the nominal geometry.

The material is assumed to be steel, with material properties defined as a piece-wise linear elasto-plastic model taken from a training example given in the Abaqus manuals [37], Table 2. Yield begins for a von Mises stress of 300×10^6 Pa, and the hardening is defined linearly in each stress range. The limiting strain defined in this model is 0.35, occurring at a stress of 400×10^6 Pa; however for this model element deletion is not applied for stresses exceeding this value – in order words, elongation to failure and fracture strength are not considered in the material model. Note that the applied pressure loading gives rise to a nominal uniaxial stress of 270×10^6 Pa, which is within the elastic regime. This is a simplistic model, and for the purposes of this current paper, modelling of dislocation plasticity and crack initiation are out of scope. A basis for inclusion of these effects is given by Brinckmann and Giessen [38] in their study of crack initiation at rough surfaces.

Table 1. Model information.

Parameter	Value	Unit
Gauge diameter of specimen	4×10^{-3}	m
Gauge height	1×10^{-3}	m
Surface roughness band height	80×10^{-6}	m
Typical surface roughness size	$< 8 \times 10^{-6}$	m
FEA mesh seed size in the surface roughness region	0.25×10^{-6}	m
FEA global mesh seed size	20×10^{-6}	m
Applied pressure load, equal to nominal uniaxial stress state	$\pm 270 \times 10^{6}$	Pa

Table 2. Material data.

Elastic properties		Plastic properties	
Young's Modulus (GPa)	Poisson's ratio	Stress (MPa)	Strain
210	0.3	300	0.0
		350	0.025
		375	0.1
		394	0.2
		400	0.35

Before turning attention the effect of the surface roughness, it is worth considering the simple calculation of the stress within the specimen. Let us compare two specimens: the perfect specimen with a cross sectional radius of 2 mm, and another smooth specimen, but with a cross sectional radius of 1.992 mm, reduced by the maximum typical surface roughness of 8 μm. This is thus the nominal surface as defined in Section 2.4.

In both cases, the stress state is uni-axial, and the applied load is the same. The stress in the perfect specimen is 270 MPa, but the stress in the other is increased by the square of the ratio of the two specimen diameters:

$$\text{stress in smaller specimen} = 270 \times \left(\frac{2}{1.992}\right)^2 \cong 272.2 \text{ MPa} \qquad [6]$$

This gives an increase of less than 1% in the stress, and is therefore still below 300 MPa, the yield stress. The effect of surface roughness is far more significant that the effect it has on nominal dimensions.
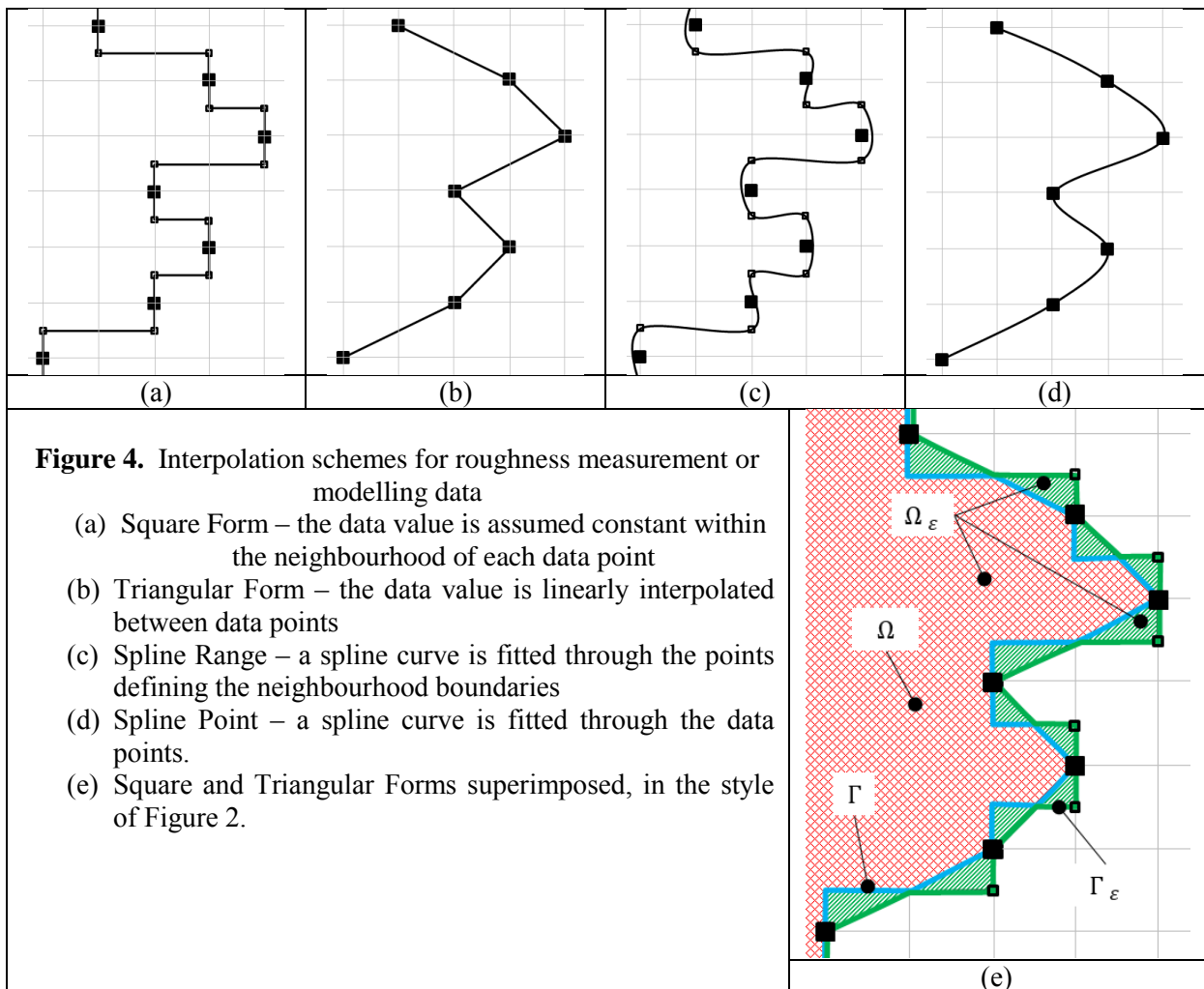
3.2. Interpolation schemes

In the measurement of surface profile, the results would typically be tabled from a grid of positions on the surface, with surface height relative to a datum. In the axi-symmetric case, these can be shown in two dimensions, see Figure 4, where position on the surface is shown vertically, and profile height is shown horizontally from the left. The large squares indicate measurements. With no further measurement information, the question is then how to choose what form of interpolation to adopt, and whether that choice is important.

Four of the most obvious interpolation schemes are illustrated, and presented in Figures 4 (a), (b), (c) and (d). Figure 4 (e) shows the superposition of the square and triangular forms from which an "outer" and an "inner boundary" can be drawn. By comparison with Figure 2, these two boundaries define two similar domains, for which the results of a linear elastic stress analysis should differ no more than the limiting value prescribed by Theorem 0.1. Since both interpolation schemes lie on or within these two boundaries, the differences between their stress analysis results should also be within that limiting value. The same argument can be applied to the other two interpolation schemes. Note, however, that Theorem 0.1 is not necessarily true for results where the yield stress has been exceeded.

In reality, the actual surface pattern depends on the manufacturing processing, and on the grain size and structure of the material relative to the machining cut size [39]. While it is probably the case that the triangular form is the more representative, by exploring different interpolation schemes we intend to show later in the paper that the choice of form is not as significant as the range and frequency of

variation. For the majority of the work presented in this paper, the square form (a) is adopted, as for this form, complete uniformity of the finite element mesh can be ensured.

A deeper question concerns the effect of surface profile variation at a smaller length scale than is observable at the surface grid spacing. In this paper, this effect is considered by investigating the effect of multiple scales of surface roughness. A subsequent question concerns the effect of grain size, that is, the effect of the heterogeneity of grain stiffness and orientation, where the grain size is of comparable size to the surface roughness features. This latter question will be addressed in future work.

Figure 4. Interpolation schemes for roughness measurement or modelling data
(a) Square Form – the data value is assumed constant within the neighbourhood of each data point
(b) Triangular Form – the data value is linearly interpolated between data points
(c) Spline Range – a spline curve is fitted through the points defining the neighbourhood boundaries
(d) Spline Point – a spline curve is fitted through the data points.
(e) Square and Triangular Forms superimposed, in the style of Figure 2.

3.3. Finite Element Modelling

All the finite element analysis results presented in this paper were obtained using Abaqus Standard version 6.14-1. The mesh employed in the region near the rough section of the boundary was a high density quad (CAX8R) mesh: and wherever applicable, this region is meshed with a regular array of square elements. Away from the surface roughness region, the element size and shape is less significant, and occasionally CAX6 triangular elements were employed. The basic meshing strategy adopted is illustrated in Figure 5. The global seed size was set to 20×10^{-6} m, and edge seed sizes in the regions around the surface roughness region were set to 0.25×10^{-6} m. Care was taken in

partitioning, edge seeding and choice of meshing technique to ensure high quality meshing in the surface roughness region.

Figure 5. Meshing strategy.
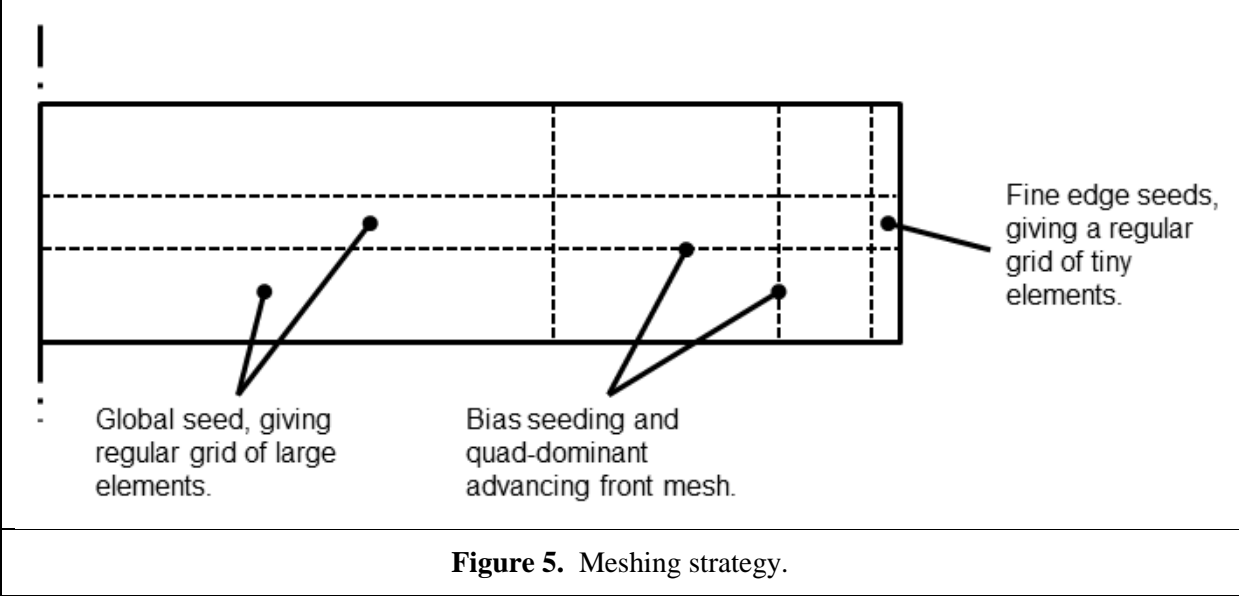
Results for von Mises stress throughout this paper are plotted using contour bands representing the piecewise linear stress ranges. Results for plastic equivalent strain (PEEQ) are plotted on a logarithmic scale from 0.1 down to 10^{-7}. Legends for both scales are shown in Figure 6, with the von Mises stress values given in MPa.

Where practical, the mesh lines are shown, but in all cases the plot style is "quilt", so that the stress or PEEQ value within a single element is indicated by a single colour. This means that, for analysis results presented for regions of high mesh density, the pixilation of colour is indicative of the mesh refinement.

Figure 6. Legends for analysis results: (a) von Mises stress results (MPa), (b) PEEQ results
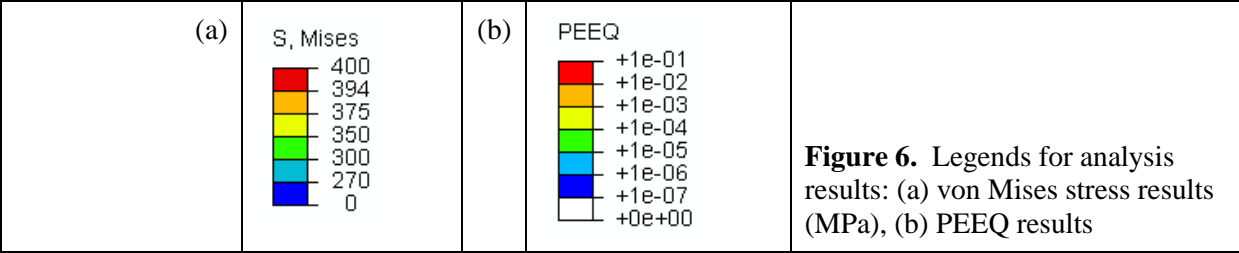
4. Systematic representation of surface roughness

4.1. Representation of surface roughness using fractals

Initially, to have a systematic approach to modelling surface roughness, the Minkowski sausage form was employed at two scales, Figure 1(a) and 1(b), and in combination, Figure 1(c). In all three cases, the grid square length illustrated in Figure 1 is 0.25×10^{-6} m, such that there are 20 repeats of styles (a) and (c) within the 80×10^{-6} m gauge length, and 80 repeats of style (b).

Since the features shown in (a) and (b) are simply different in scale, and both are much smaller than the overall test geometry, comparison of analysis results should only reveal mesh-scale effects. To explore the notion of surface roughness complexity, the results obtained from geometries (a) and (c) are then compared, Figures 7 and 8.

4.2. Results showing effects of surface roughness on the near boundary stress-strain state

For a perfectly smooth test geometry, the applied loading would equate to a uniform von Mises stress state of 270×10^6 Pa throughout. In the case of the rough geometry, well away from the boundary region, this same nominal stress state is observed; however, the surface roughness features have the effect of influencing the stress distribution, Figure 7. Although the nominal stress state is below the yield stress for the material, some regions close to the surface roughness features exhibit stresses in excess of the yield stress.

In Figure 7, the boundary between the dark and light blue represents stress at exactly the nominal stress; dark blue represents lower stresses and light blue stresses between nominal and yield. Green represents stresses above yield. Figure 8 shows the equivalent plastic strain (PEEQ) results. Regions below yield are shown in pale grey, while PEEQ values above 1×10^{-7} are shown on a logarithmic scale. NB: the legends for Figures 7 and 8 (and all subsequent figures showing von Mises stress and PEEQ contour plots) are given in Figure 6.
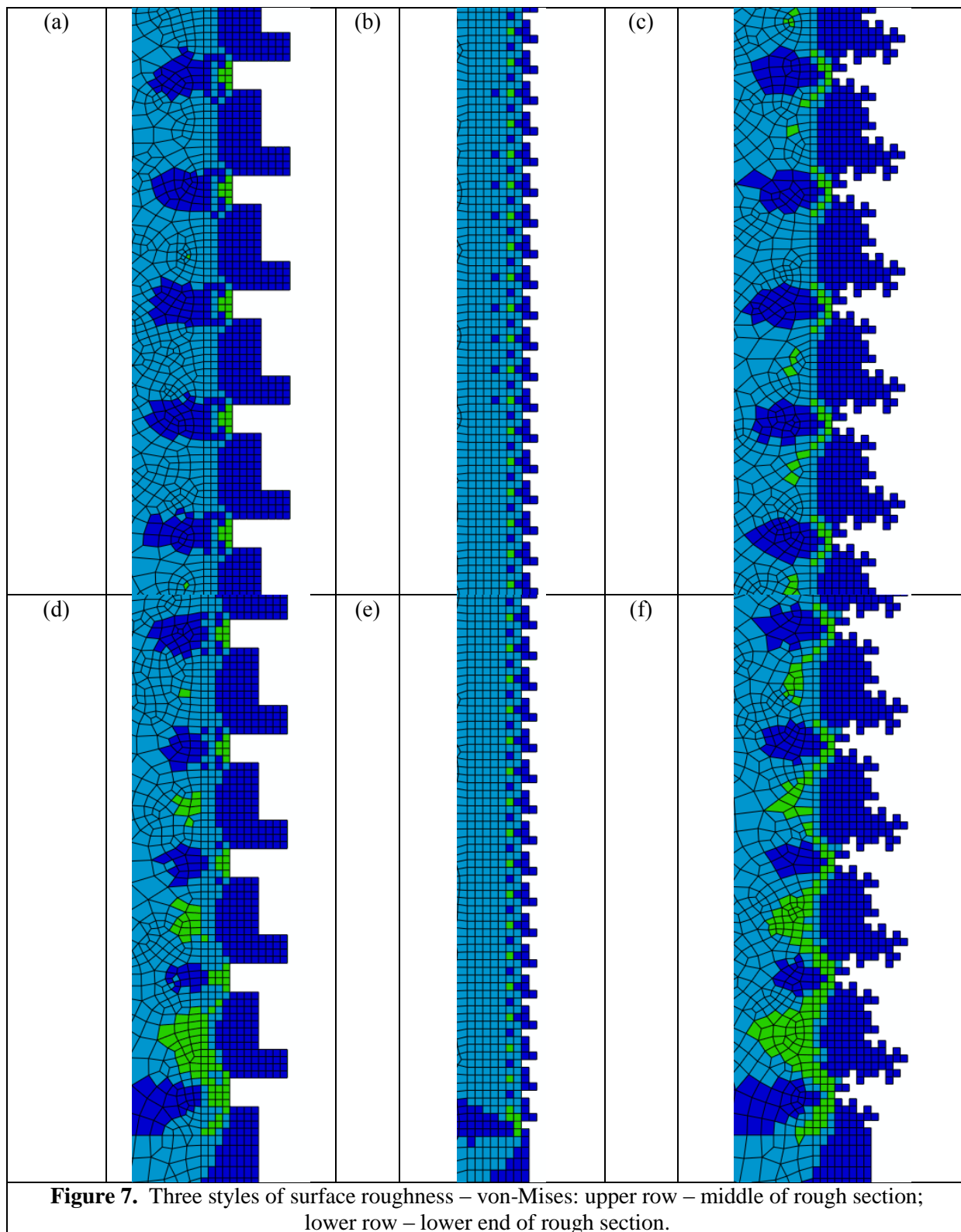
Since the surface roughness features are applied to only a part of the boundary, it is reasonable to think that the stress-strain state shown in the middle of this surface roughness section should be representative of the stress-strain state where the complete surface had that same roughness, Figures 7 and 8 (a, b and c). The results for (a) and (b) are similar and to scale, as anticipated. Comparing von Mises stress results, Figure 7(a) and (c), there is some clear similarity at a distance from the surface feature, but close to the surface other features are observed. The PEEQ results show regions of similar sizes, but the positions of the regions with higher levels of PEEQ are determined by the finer detail surface roughness.
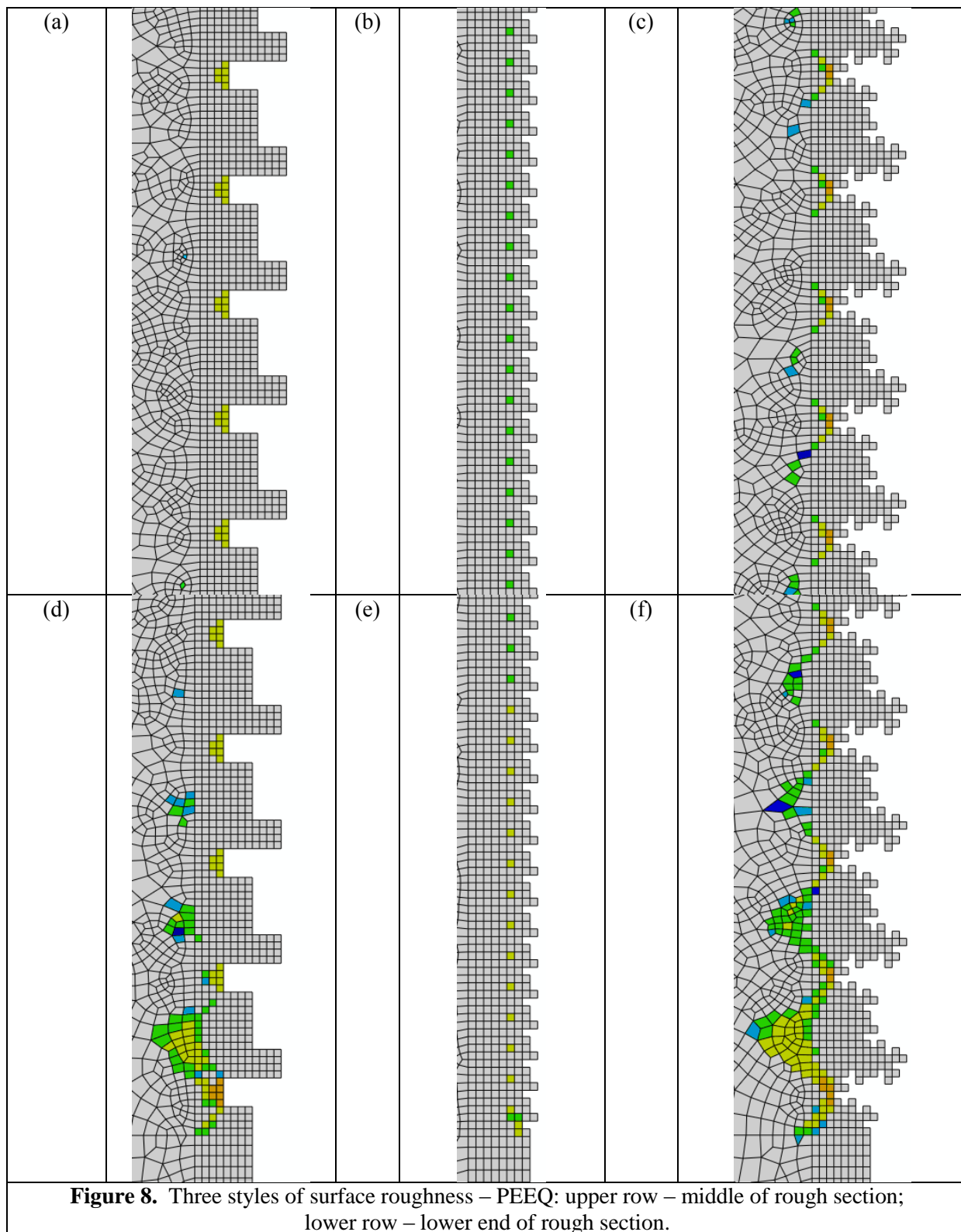
It is also interesting to observe the stress-strain state where the surface roughness section transitions abruptly to the smooth geometry, Figures 7 and 8 (d, e and f). Notice that the size of the PEEQ regions increase and the levels of PEEQ within those regions are also higher. This transition effect seems to extend over a region of about three repeat feature lengths.
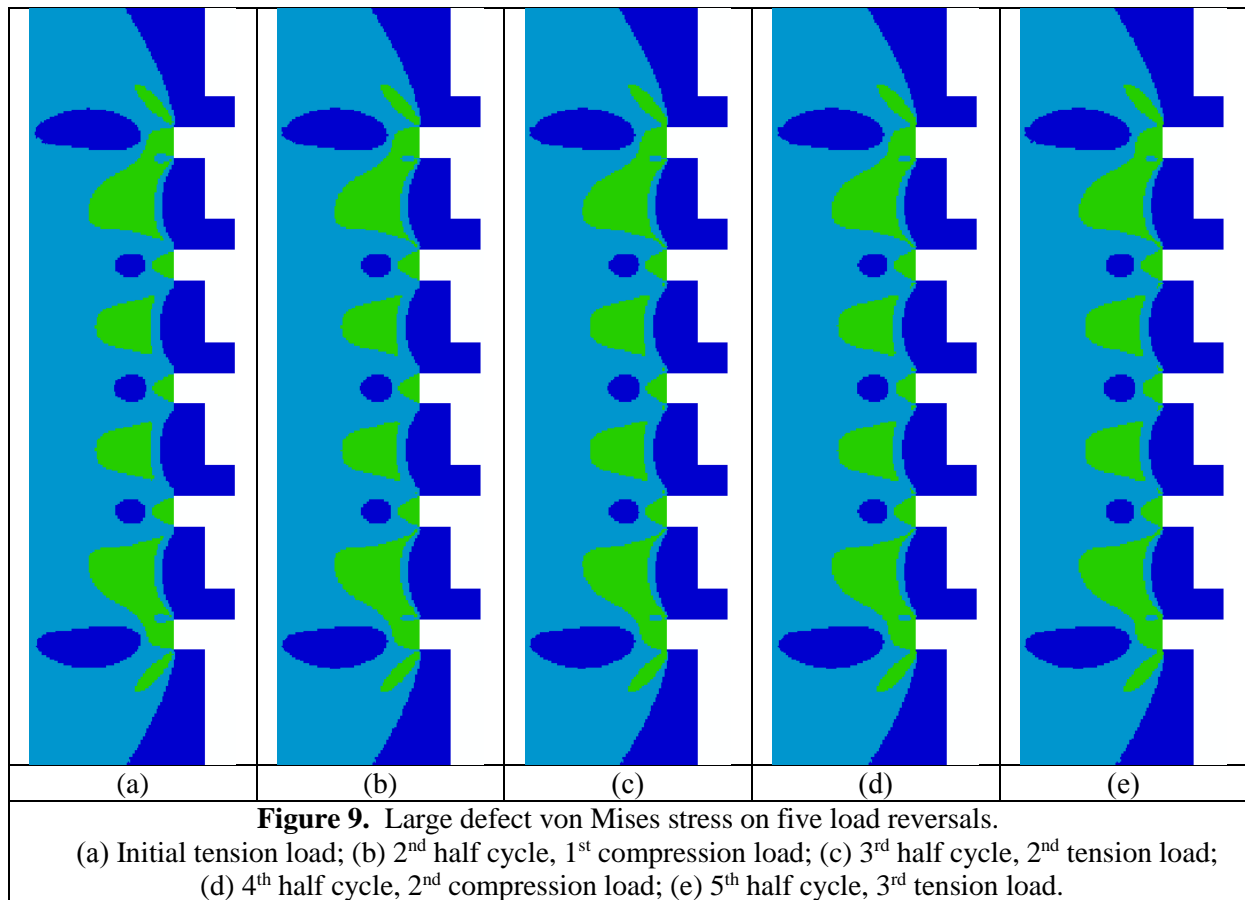
5. The effect of repeated loading

The results presented in Section 4 demonstrated that surface roughness can lead to local regions of plastic deformation. In this section the effects of repeated fully reversed loading are explored.

The load cycles were applied as a sequence of Steps (in Abaqus), first in tension and then in compression, so that during each half cycle the nominal von Mises stress is 270×10^6 Pa.

Figure 7. Three styles of surface roughness – von-Mises: upper row – middle of rough section; lower row – lower end of rough section.

Figure 8. Three styles of surface roughness – PEEQ: upper row – middle of rough section; lower row – lower end of rough section.

| (a) | (b) | (c) | (d) | (e) |

Figure 9. Large defect von Mises stress on five load reversals.
(a) Initial tension load; (b) 2nd half cycle, 1st compression load; (c) 3rd half cycle, 2nd tension load;
(d) 4th half cycle, 2nd compression load; (e) 5th half cycle, 3rd tension load.

5.1. Test geometry with five simple surface roughness features

The geometry used here is again similar to that used before, but scaled up by a factor of four. In order to obtain high resolution results, the same 0.25×10^{-6} m square mesh size is adopted.

The surface roughness feature length is 16×10^{-6} m, equal to 64 elements' length. To be able to present data with such a high fidelity mesh it has been necessary to suppress the mesh lines, but the presentation style is "quilt", so in Figures 9 and 10 each square element is effectively a single pixel of colour.

The results for von Mises stress (Figure 9) show very little obvious change with increasing number of load reversals, except near the surface, on very careful inspection. The PEEQ results (Figure 10), are more useful, and indicate that the outer boundary of the plastically strained material remains constant. Plotting PEEQ for much smaller values, not presented here, made no discernible difference, so it would seem that the plasticity remains regionally confined. Within the plastically strained region the level of PEEQ gradually increases, either from the boundary inwards, or radially from the centre of regions that are fully internal.
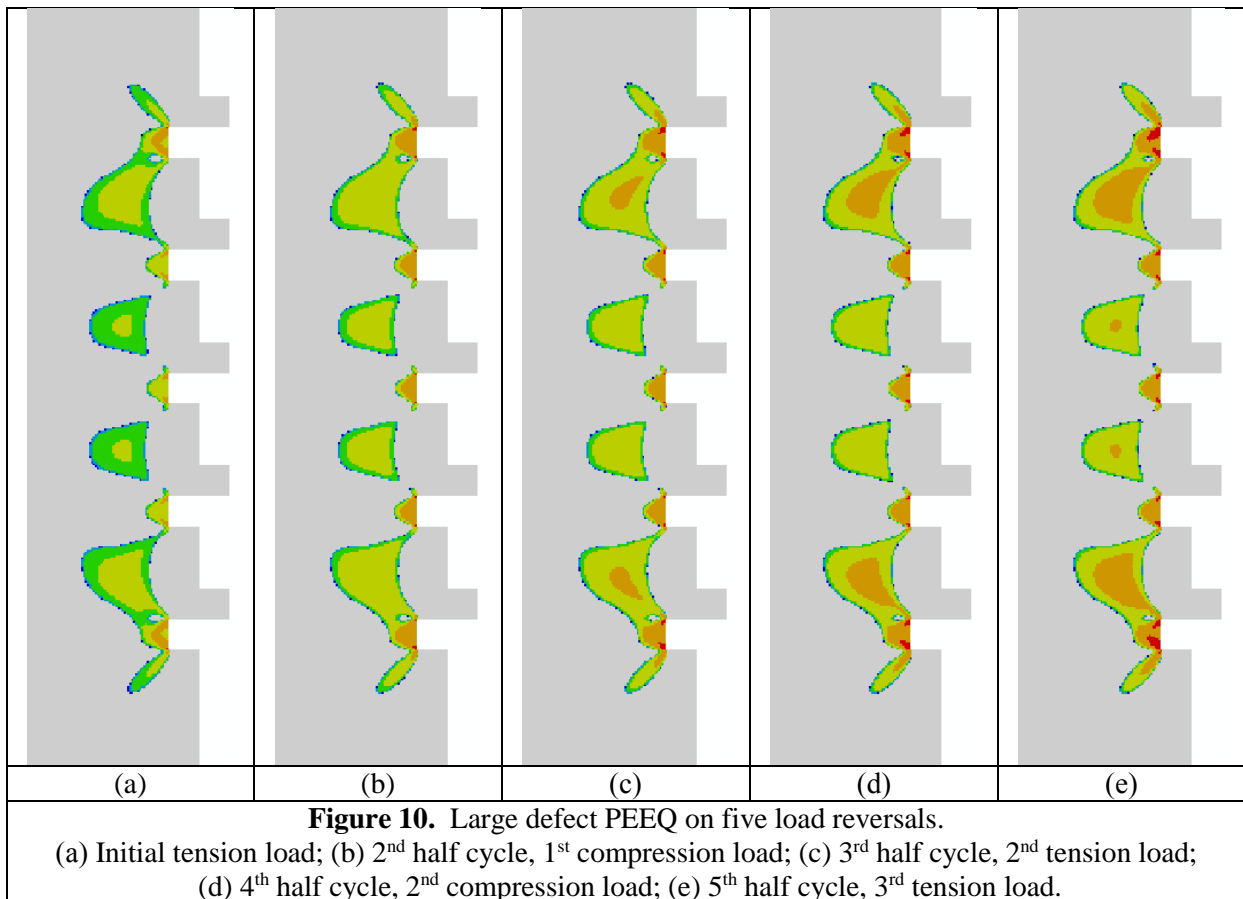
5.2. Specimen with a large irregular defect

The test case considered here modifies the surface roughness type as shown in Figure 7(c) to include a larger scale surface roughness feature, with feature length 16×10^{-6} m: i.e. third order Minkowski sausage geometry. The same 0.25×10^{-6} m regular grid meshing strategy was employed as before.

The same five load reversals were applied, and the results presented in Figures 11 and 12. In Figure 11(c) and (d), notice that the light blue region, representing stresses above nominal, but below yield, has expanded, compared with that in Figure 11(a) and (b). Also note that the oval lobes of green

have become slightly shorter and wider. These are relatively small effects, indicative of some stress redistribution.

The more interesting effects can be seen in Figure 12. Notice how the boundary of the region containing plastically strained material, *i.e.* non-zero PEEQ values, remains constant, while plasticity levels grow within the region. Notice also that the extent of this PEEQ region is about twice that of the length scale of the defect in both depth and breadth.

| (a) | (b) | (c) | (d) | (e) |

Figure 10. Large defect PEEQ on five load reversals.
(a) Initial tension load; (b) 2nd half cycle, 1st compression load; (c) 3rd half cycle, 2nd tension load;
(d) 4th half cycle, 2nd compression load; (e) 5th half cycle, 3rd tension load.

6. Effect of surface profile interpolation method

The geometries used in Sections 4 and 5 were based on a square form interpretation of a notional surface roughness measurement set. Insisting on a square form was convenient, as this meant that all elements in the region of significance would be identical in shape and size. With alternative interpolation schemes the guarantee of mesh size equivalence is much harder to meet; however, the results shown Figures 7 and 8(d) and (e) and Figures 9 and 10(a) indicate that similar distributions are obtained for different scales of model, so it might be reasonable to expect results to be reasonably mesh size independent.

On that basis, the regular case as studied in Figures 7 and 8(a) and (d) was re-drawn using the alternative interpolation schemes as illustrated in Figure 4. The more interesting and revealing results are those for PEEQ, for the initial loading case and for the 5th half cycle (Figure 13).

Notice that although mesh seed sizes employed were broadly equivalent for the meshing of each geometry, the resulting meshes are somewhat variable in mesh density. The size of the elements, and their orientation and conformity to the PEEQ distribution does seem to have an effect; however, the results obtained suggest that PEEQ distribution is largely independent of the interpolation used.

7. Modelling of random surface roughness

7.1. Comparison of interpolation schemes
The purpose of examining particular features and systematic combinations of features is to understand what is important and significant in the modelling of surface roughness. While a fractal approach like the Minkowski sausage provides a systematic method for creating details within details, it does not actually create a realistic looking surface roughness profile. On the other hand, it is clear that the relative periodicity of the largest surface roughness feature size determines the approximate penetration depth of the plasticity region within the material.

In the final test cases presented in this section, a random surface roughness profile was generated, according to an algorithm. The surface roughness region, of length 80×10^{-6} m, was divided into 80 regions of length 1×10^{-6} m, 40 regions of length 2×10^{-6} m, 20 regions of length 4×10^{-6} m, and 10 regions of length 8×10^{-6} m. Padding regions at the top and bottom of the surface roughness region of length 8×10^{-6} m were defined, enabling a further division for the middle 64×10^{-6} m into four regions of length 16×10^{-6} m, two regions of length 32×10^{-6} m and one region of length 64×10^{-6} m. Each of these regions defines a periodicity of surface roughness, and an offset from the nominal geometry can be defined for each region.

To create the geometries shown in Figures 15 onwards, the offset was defined randomly, with the probability given in brackets: $+ 1 \times 10^{-6}$ m (0.25); 0 (0.5) and $- 1 \times 10^{-6}$ m (0.25). For each position on the surface of the test geometry, the total offset is the sum of the offsets for each region for which that position is a member. This principle is illustrated in Figure 14.

7.2. Extended load cycles
In the results presented so far, it can be seen that the plasticity region is localized and remains almost constant during load cycling. The level of plasticity within that region does, however, increase.

Figures 18 show the effect of increasing the number of cycles, at the 1st, 2nd, 5th and 10th tensile load application. The elements coloured black in Figure 18(d) indicate PEEQ values exceeding 0.1. The overall PEEQ values grow more slowly with increasing numbers of load cycles, but with such high levels of PEEQ it is probably unreasonable to develop the analysis further without considering other material failure effects.

8. Discussion
The results presented here explore a range of subtly different issues, so it is appropriate to review these findings as a whole, and then to consider particular aspects.

8.1. Relationship between surface roughness feature size, regularity and "zone of influence"
Each of the analyses results presented here indicate that the size of a surface roughness feature has a significant influence on the extent of the region affected by higher than nominal stresses. Because of the choice of applied load level and elasto-plastic material model, the resulting zone of non-zero PEEQ provides an unequivocal measure for what might be described as the "zone of influence" for the surface roughness feature.

The regularity of the surface roughness feature is of importance. In each case, the largest "zone of influence" effects are seen in the location of an isolated feature, or at the transition from the smooth boundary to the central band where the surface roughness is applied.

In Figures 7 and 8 we see that the size of the PEEQ zone is similar to that of the height variation and extent of the surface roughness feature. In Figures 7(f) and 8(f), it is the larger scale feature which is important: the smaller scale feature changes the shape and some details of the PEEQ zone near the boundary, but the area and extent is similar to the equivalent result shown in Figures 7(d) and 8(d).
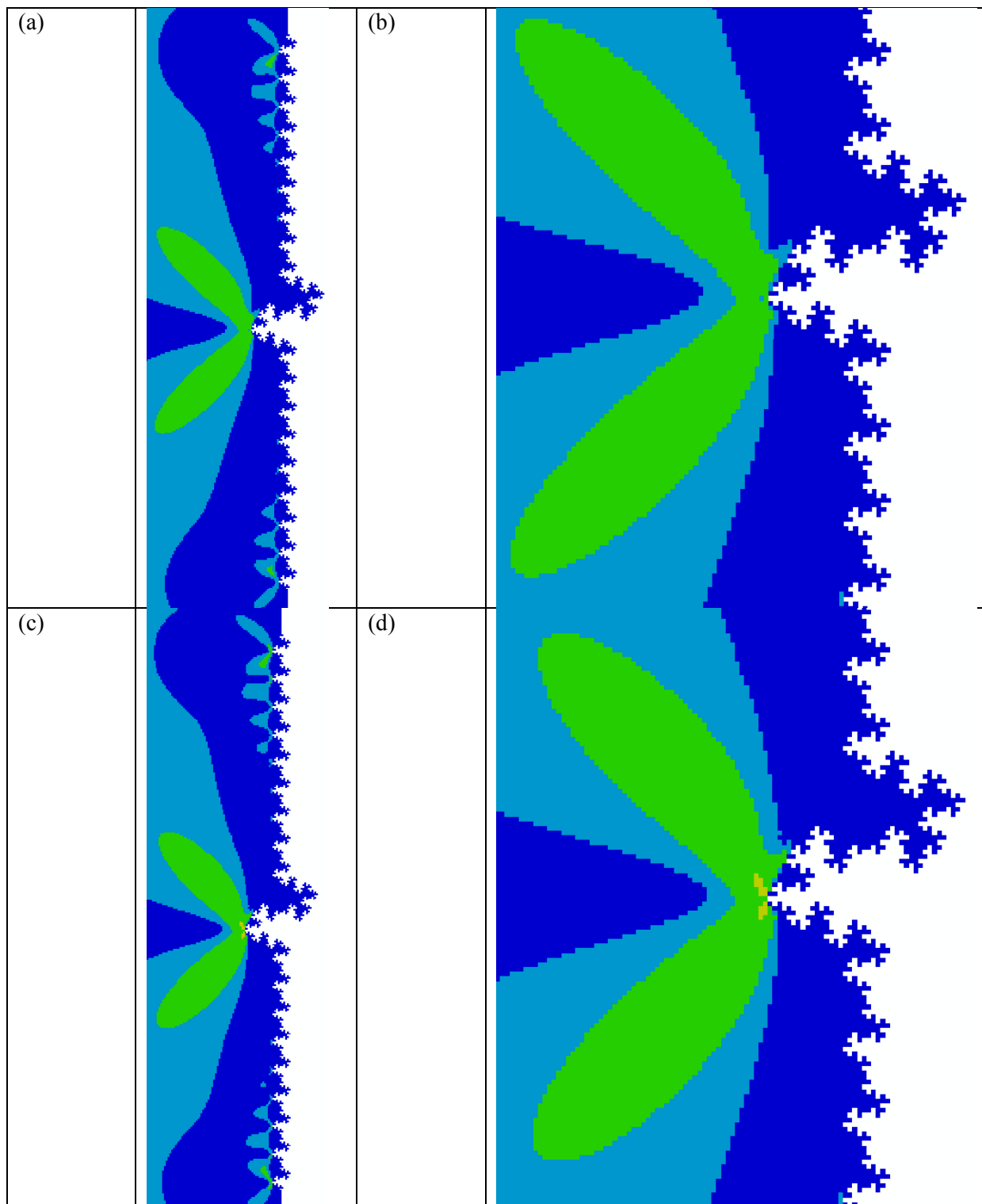
Figure 11. Irregular large defect: von Mises stress at first and fifth load reversals. (a) Initial tension load, full surface roughness region; (b) zoomed view; (c) 5th half cycle, 3rd tension load, full surface roughness region; (d) zoomed view.
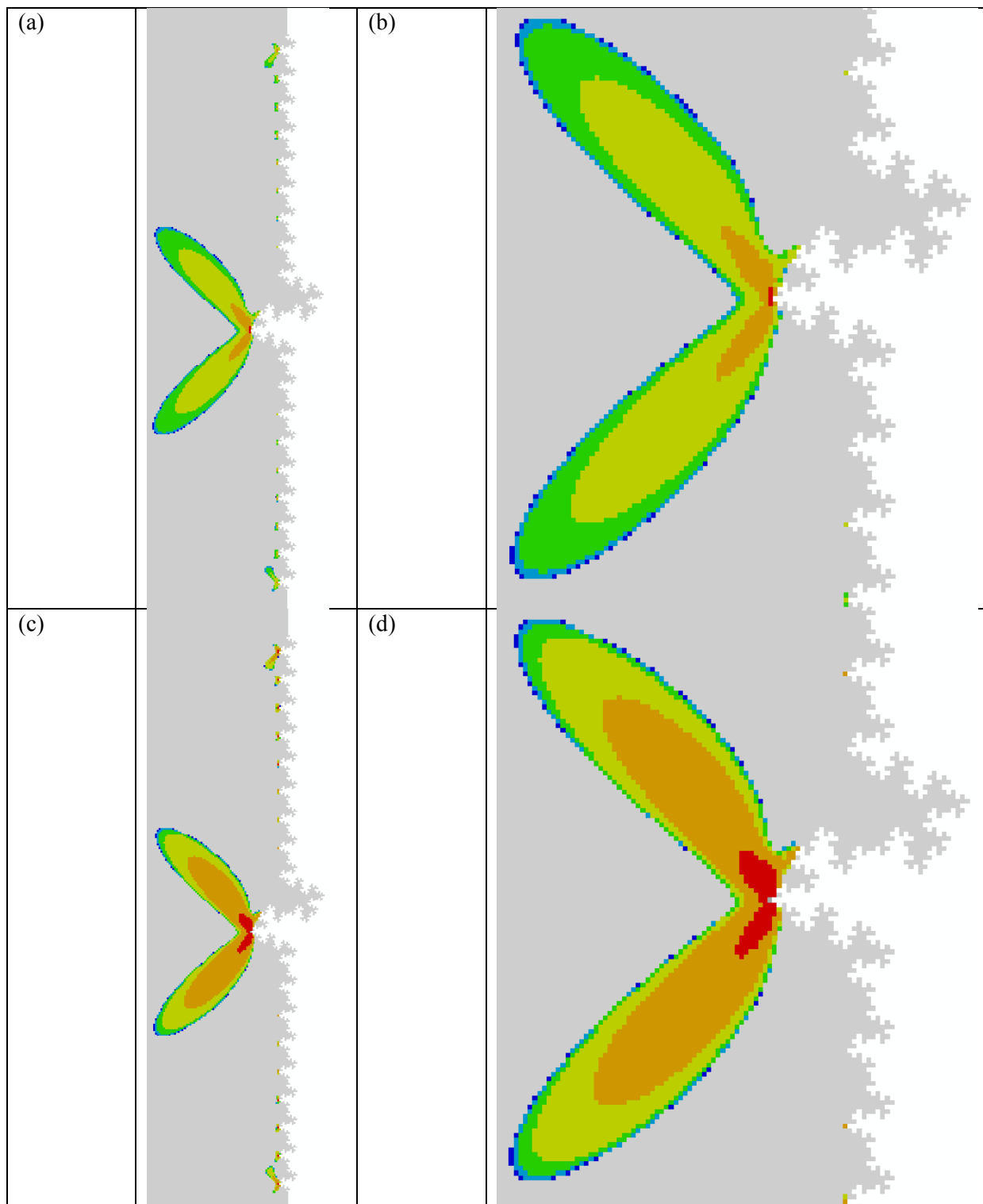
Figure 12. Irregular large defect: PEEQ at first and fifth load reversals.
(a) Initial tension load, full surface roughness region; (b) zoomed view;
(c) 5th half cycle, 3rd tension load, full surface roughness region; (d) zoomed view.
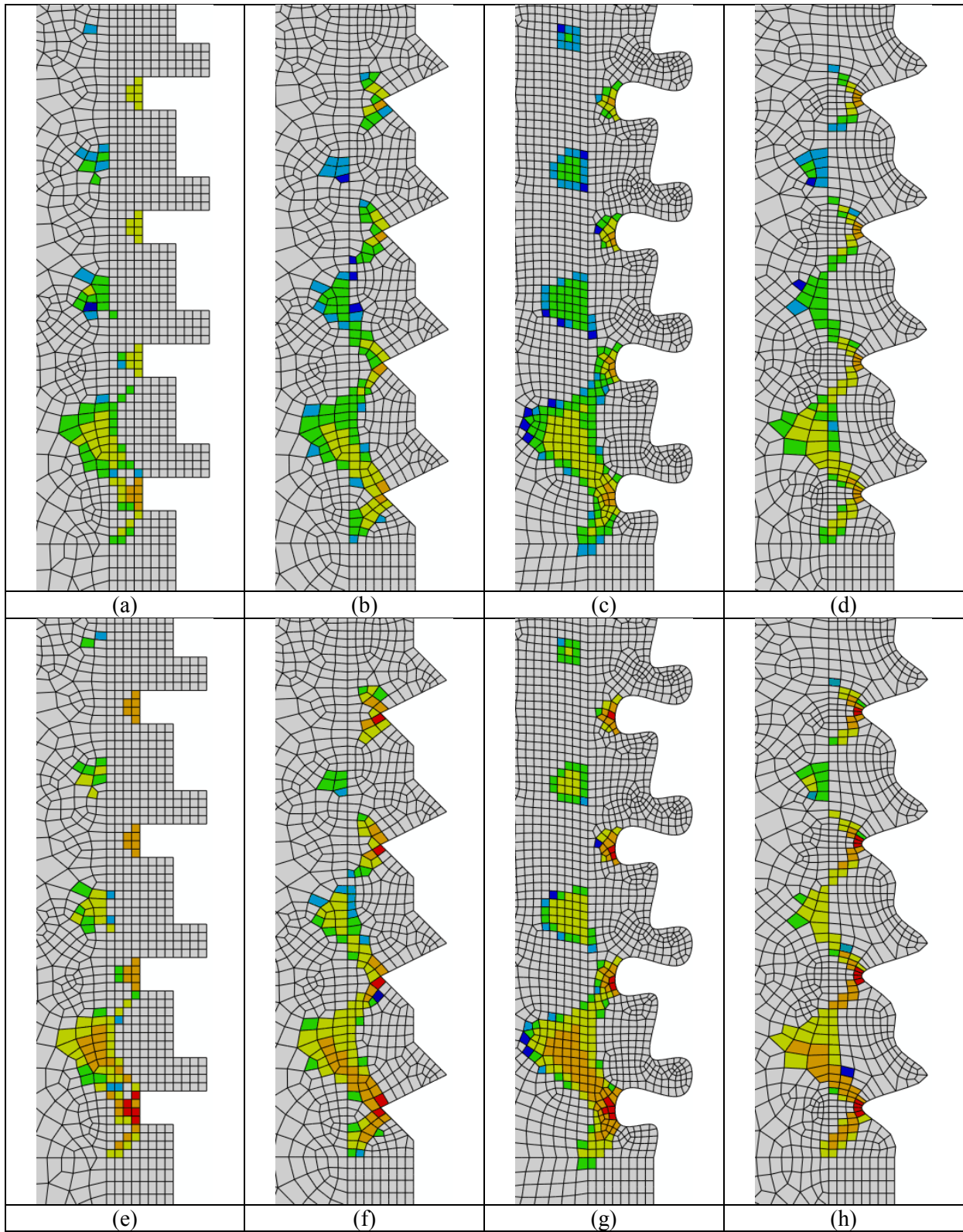
Figure 13. PEEQ, regular surface roughness, various interpolation schemes, first tensile and fifth load reversal.

First tensile: (a) Square form; (b) Triangular form; (c) Spline range; and (d) Spline point

Fifth reversal: (e) Square form; (f) Triangular form; (g) Spline range ; and (h) Spline point

In Figures 11 and 12, the main feature displayed is a three level feature embedded in a region comprised of an otherwise regular set of two level features. In this case, the result is similar but depth of the PEEQ zone into the material is somewhat larger than the height variation of the larger surface roughness feature, and the extent is also larger: in both cases by a factor of about 1.5. The same is true for the randomly generated features shown in Figures 15, particularly near the transition to the smooth boundary at the top and bottom of the central surface roughness band, where there are relatively large and relatively isolated surface roughness features; however, for the surface roughness clump which is shown enlarged in Figures 16, the extent follows the surface roughness profile quite closely to give a "sea-horse" shape with nearly square PEEQ zones.

In conclusion, the "zone of influence" is somewhat greater for an irregular surface roughness feature, but in general the extent is well defined and can be characterized by the height variation of the surface roughness feature.
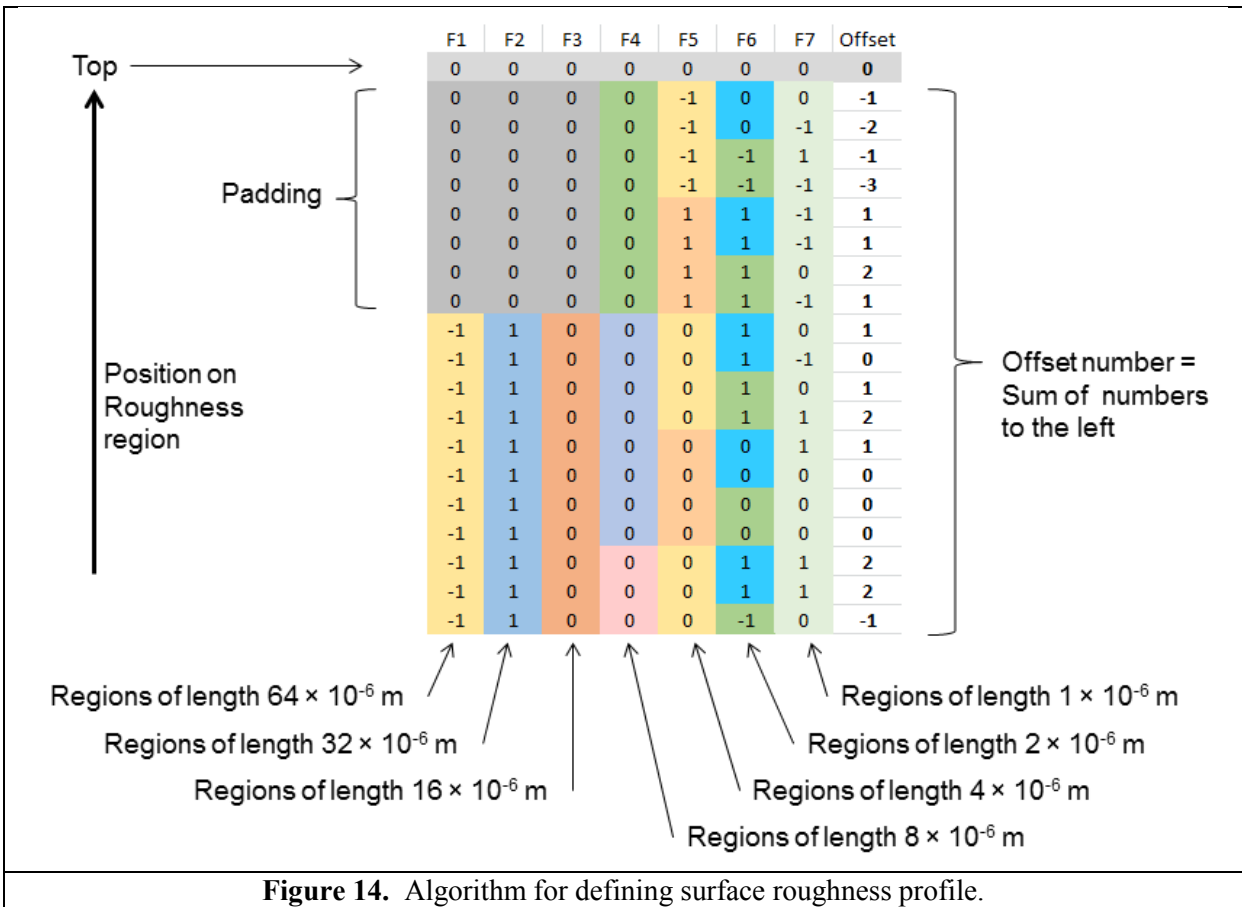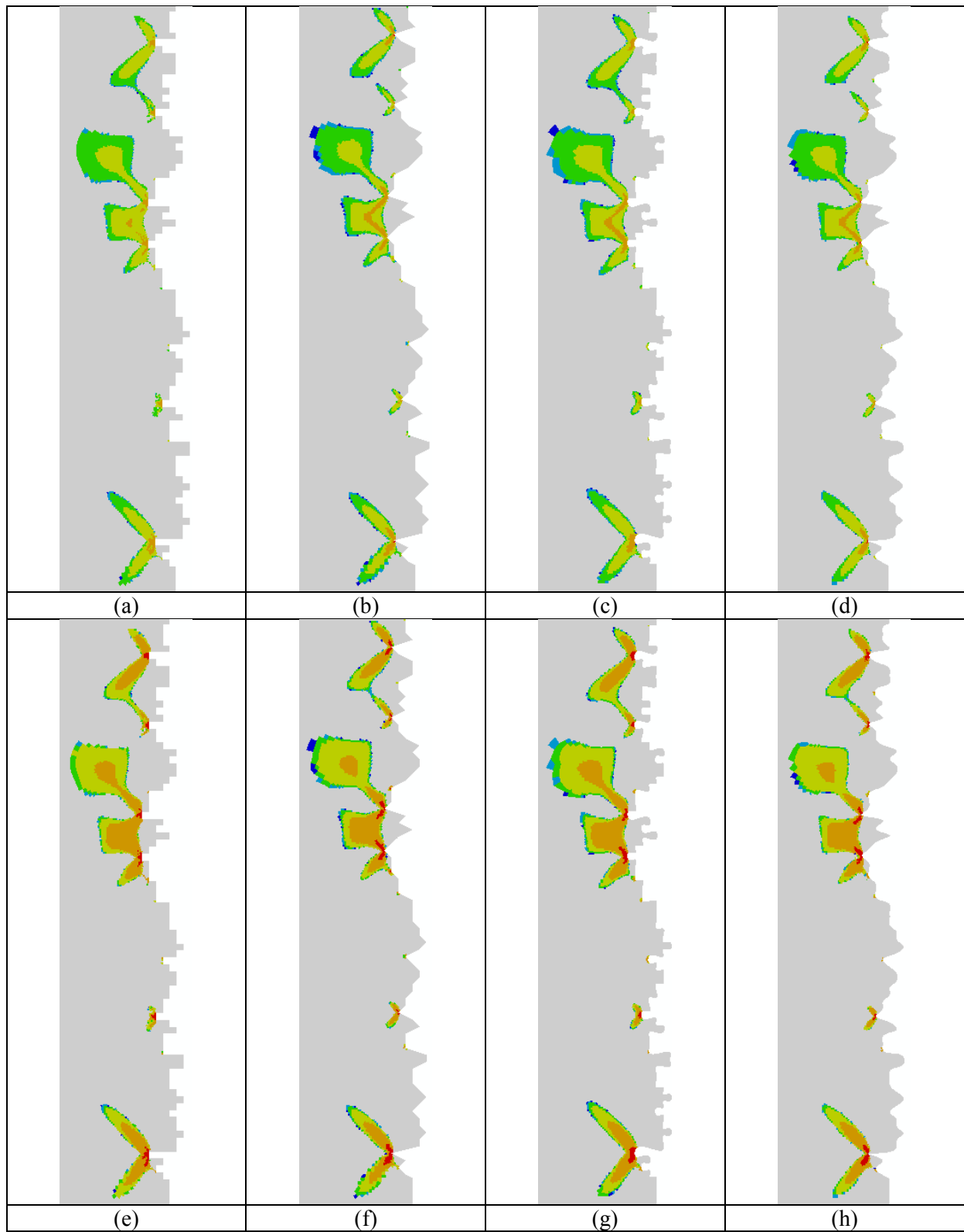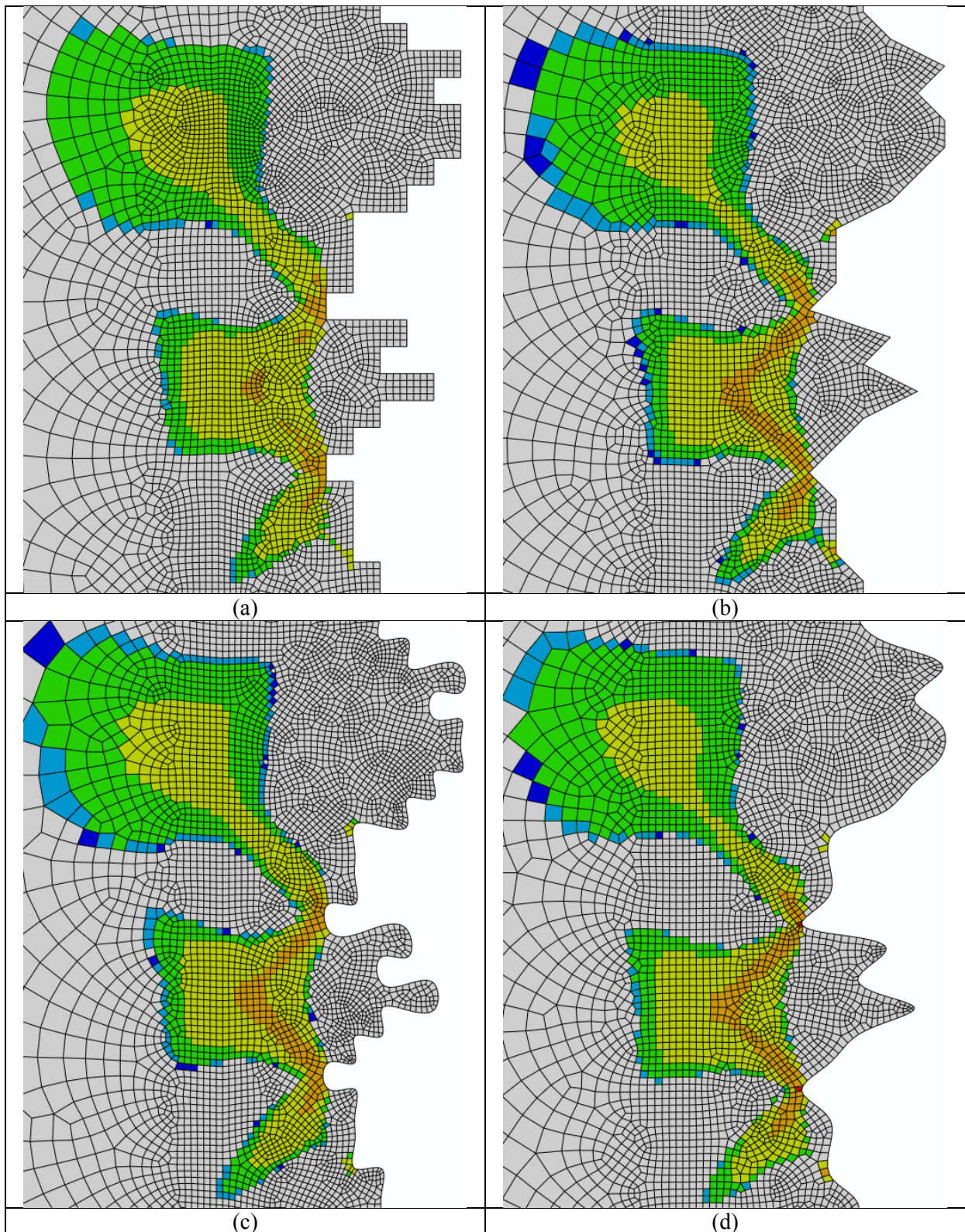

**Figure 14.** Algorithm for defining surface roughness profile.

Figure 15. PEEQ, random surface roughness, various interpolation schemes, first tensile and fifth load reversal.
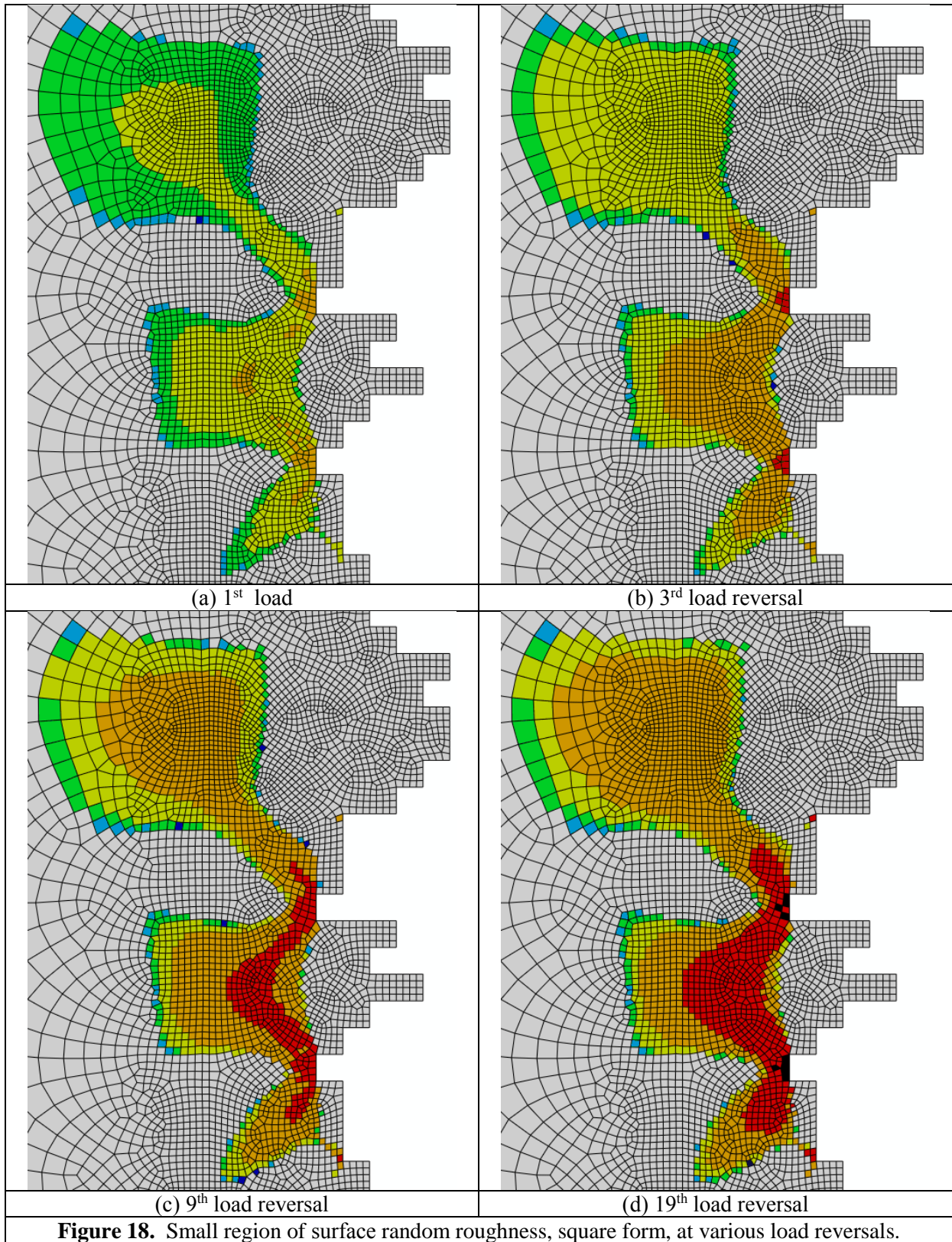First tensile: (a) Square form; (b) Triangular form; (c) Spline range; and (d) Spline point
Fifth reversal: (e) Square form; (f) Triangular form; (g) Spline range; and (h) Spline point.

Figure 16. Small region of random surface roughness, PEEQ, first tensile load.
(a) Square form; (b) Triangular form; (c) Spline range form; and (d) Spline point form.
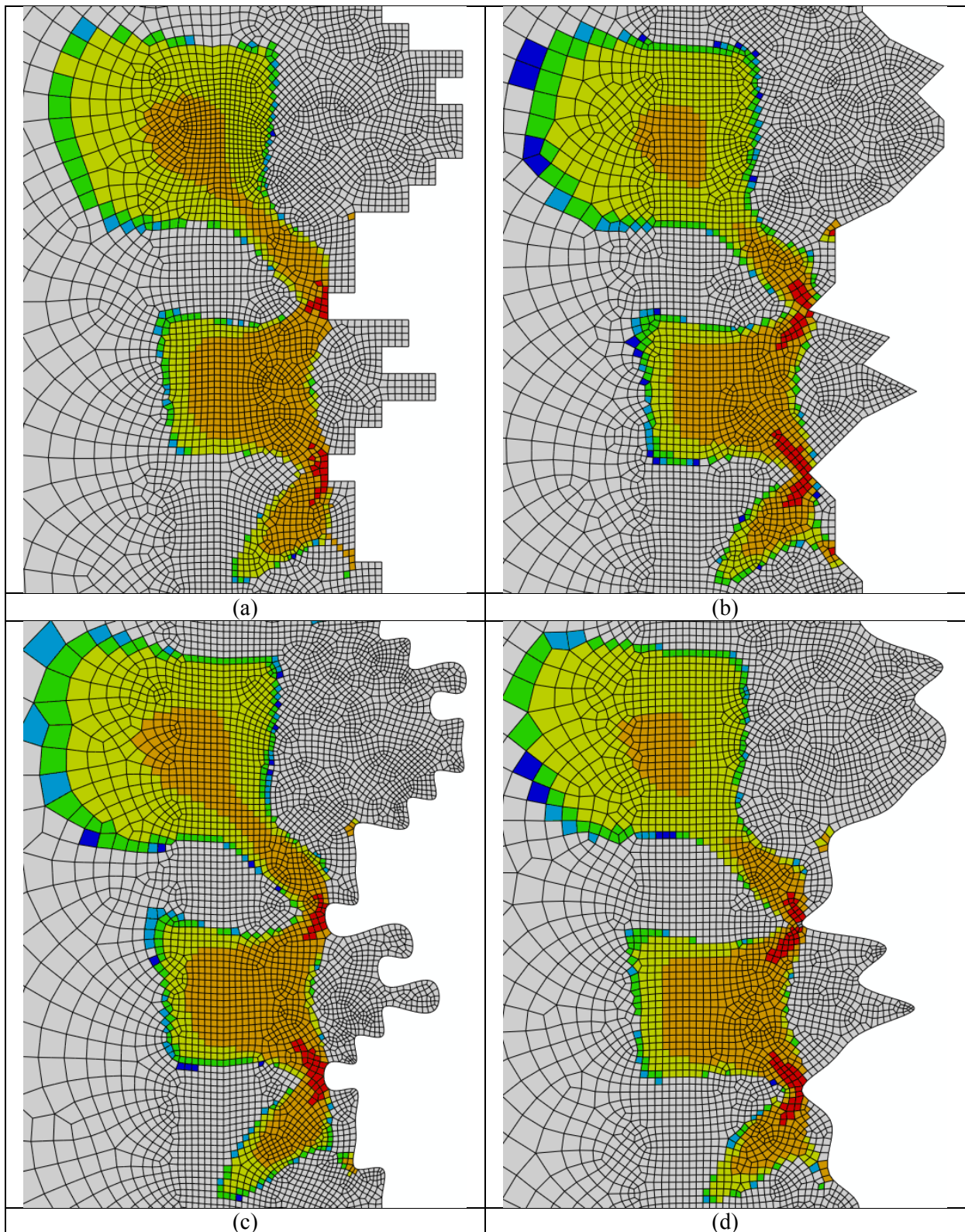
Figure 17. Small region of random surface roughness, PEEQ, fifth load reversal.
(a) Square form; (b) Triangular form; (c) Spline range form; and (d) Spline point form.

(a) 1st load	(b) 3rd load reversal
(c) 9th load reversal	(d) 19th load reversal

Figure 18. Small region of surface random roughness, square form, at various load reversals.

8.2. Effect of interpolation method

As already discussed, Theorem 0.1 suggests that for linear elastic stress analysis, the differences between the analysis results obtained using different interpolation methods for defining the boundary can be contained within a limiting tolerance. In the case of elasto-plastic analysis, when the yield stress is exceeded within a region in the model, then this defines additional internal boundaries within the model domain. In finite element analyses, these boundaries are linked to the definition of the elements, so for two identical geometries but with different meshes, these internal boundaries would be slightly different. The length scale of the boundary variations is determined by the local mesh size. Now consider the effect of the interpolation methods for describing the external boundary: until first yield, Theorem 0.1 suggests that the stress field in each model would be similar. Therefore, the locations for first yield should be similar. The question to be posed is this: do all these small variations remain small as the PEEQ region expands, or can there be substantively different developments of the PEEQ region arising only as a result of the external boundary interpolation scheme?

The results in Figures 13 are similar and suggest that the interpolation scheme is not particularly significant. There are differences in mesh density, a factor which is difficult to avoid completely, but general "zone of influence" prediction is similar, with the main differences being caused by the particular geometry at the high PEEQ region on the boundary.

The results shown in Figures 16 and 17 suggest that there is a small difference between the triangular form straight line joining of points (b) and a smooth spline point interpolation (d). The square form interpolation (a) shows the most difference to the other three forms. In all four cases, it can be seen that the regions of PEEQ that are well within the domain have similar values in similar locations. As with Figures 13, close to the boundaries, the shape of regions with high values of PEEQ do differ, as might be expected, since the choice of interpolation scheme determines whether a notch is smooth sided, blunt or a V-notch. It should also be remembered that results can also be influenced by local mesh density.

These four interpolation schemes provided methods for construction of surface profile geometry without making further inferences about surface texture or surface roughness at a smaller length scale. If one had such information, perhaps obtained by inference from another type of surface metrology method, then it would be legitimate to question further. The first issue is how to represent that within the interpolation: this would require an algorithm to add an appropriate stochastic variation onto the basic interpolation scheme. The second issue is how that level of detail would influence the "zone of influence". In answer to the second issue, observe the differences between Figures 7 and 8(d) and (f), and also Figures 11 and 12. Notice that it is the big features that dominate and the smaller ones have comparatively little influence over the majority of the "zone of influence".

In conclusion, the choice of interpolation scheme is mainly a matter for modelling convenience, as the size of the "zone of influence" is primarily governed by the largest feature size. The only significant exception to this is where there is a particular interest in the near surface region, when higher resolution modelling would be necessary. As a corollary to this conclusion, it might seem that fractal aspects in the surface profile – the scale and frequency, and in particular, fractal dimension – are less significant. Nevertheless, the nature of fractals is to add multiple levels: this work has only considered three levels. Small differences arising from smaller features, could therefore combine to give a non-negligible effect, and the relative influence of the lower level features will be related to the fractal dimension.

8.3. Effect of repeated loading

It would seem that on repeated reverse loading, the "zone of influence" remains constant, although the level of the PEEQ values increases. There is very little evidence for growth of the non-zero PEEQ zone, although that is difficult to rule out completely. In the results presented, very careful inspection will reveal that after several cycles, the zone might expand by one element on part of the zone

boundary, for example compare Figure 18(b) and (c), but a very much finer mesh would be required to make any conclusive judgement on this.

Although it is tempting to think of this as a model for fatigue, this modelling method does not lend itself to very large numbers of load reversal. As the PEEQ values increase, it should be remembered that the material model is of limited applicability, and it would probably be appropriate to introduce failure mechanics into the model.

The highest values for PEEQ are observed at the surface boundary where the surface roughness flaw is at its deepest, and these regions connect up with neighbouring ones, in a wavy band formation which is approximately a smoothed mirror image of the surface profile. Given that the increasingly high values of PEEQ represent regions of material where plastic slip zones have been activated and reversed, this suggests material that is beginning to be pulled apart. In reality, under such working, porosity would be growing within the material, which would then be subject to environmental aging. In view of this, the modelling results might be interpreted to provide some understanding of the process of corrosion-fatigue and corrosion pit formation. If elements in the model were deleted on reaching a particular level of PEEQ, then would that result in failure following the wavy band path, and result in flaking and corrosion pitting?

In this context, it should be noted that [40] presented a simple methodology that uses measured surface roughness, in conjunction with the Hartman-Shijve crack growth equation [41], for accurate computation of both the fatigue life and the crack growth history associated with a test on a corroded bridge steel specimen. This methodology has the advantage that it captures the total fatigue life, not just the time to initiation.

8.4. Computational modelling considerations

Finite element method is a robust general purpose tool for modelling a wide range of problems, and it is because of the capability and commercial development of packages such as Abaqus that the analysis presented here was carried out as conveniently as it has been. Notwithstanding this, finite element does not lend itself particularly well to the problem: most of the problem domain is uninteresting, but it is difficult to generate efficient meshes that capture the surface roughness regions in sufficient resolution and then to manage a mesh transition through a factor of about 100. While this can be done for a simplistic 2D axi-symmetric geometry, as presented here, it would not be convenient for a more complex specimen shape.

More sophisticated meshing tools exist than used in this present work, as do commercial finite element packages which include automatic mesh refinement. These might suggest an appropriate approach; however, the *modus operandi* of these tools is that of practicality for "normal" engineering analysis problems, and controlling exact element sizes and mesh formations in one region, and forcing a particular mesh transition is a requirement not anticipated by the developers of the packages. This means that model preparation is time consuming: acceptable for research purposes, but not for routine application.

Now suppose that the ideas presented here are adopted by industry and a stress engineer needs to assess the effect of surface roughness on a complex component. The technique of adding surface roughness geometry to the main component model would be, at best, inconvenient. The surface profile height variation should provide a first estimate for the depth of the "zone of influence", and this would enable appropriate model partitioning, such that mesh sizes for the geometry details and for the plastic zone would be appropriate. A further computational saving could be made by setting all material outside of the "zone of influence" to be linear elastic only, since it should only see a stress state in the elastic regime.

Despite the fact that these steps are all possible, the industrial stress engineer wants a more automated approach: so this is the right time to be considering which computational methods and algorithms lend themselves to a more effective solution to the problem. Options which present themselves include: (i) a finite element model of the basic geometry, with a refined mesh substructure to capture the surface profile and plastic zone; (ii) a finite element model of the basic geometry, with a

meshless enrichment zone approach to capture surface profile, plastic zone and potential crack growth; (iii) a boundary element model of the complete geometry with defined elasto-plastic zones, (iv) a boundary element model of the complete geometry, with a finite element model of the "zone of influence" running under co-simulation, or (v) a user element encoding the mathematical correction term as described in Section 2.3. Other permutations are also possible. Each technique has advantages and disadvantages which relate to computational efficiency, model set-up convenience, and the physical attributes that can be included in the modelling.

It should be noted that, whereas the methodology discussed in this paper focuses on the role of surface roughness in the initiation process, the studies [19, 40–45] have found that for aerospace structures, the total life, including the life prior to "initiation", of operational aircraft can be determined accurately without the need to model the accumulation of the inelastic damage during cyclic loading. Nevertheless, this paper is particularly useful in that it gives a more detailed understanding of the role of surface finish on fatigue performance.

9. Conclusions

In typical finite element analysis of the stresses in an engineering component, the surface of the component is assumed to be perfectly smooth. In this work, we demonstrate that surface roughness can give rise to localized regions with significantly higher stresses state than would be predicted assuming a perfectly smooth surface. For a component comprised of ductile, elasto-plastic material and subject to a load case leading to nominal stresses at 90% of yield, there is a "zone of influence", caused by a surface roughness feature, where the stresses exceed the nominal stress by significantly more than 10% and the material strains plastically. A simplistic calculation based on a reduced nominal cross sectional area predicts an increase in stress of less than 1%. In the models presented, the "zone of influence" extends a distance from the nominal surface of the component into the body of the component which is between 1 and 1.5 times the surface roughness profile height variation.

Although a fractal representation of the surface roughness is an attractive method for representing and replicating different surface types, the size and extent of the "zone of influence" is mainly determined by the size of the largest anticipated flaw. The regularity of the distribution flaws is also a contributing factor. This concurs with the conclusions presented in [44, 45]. Further work, exploring the effect of multiple fractal levels and comparing directly with interpolation schemes could shed more light on this.

The analysis methods presented here can be applied to repeated reversed loading. In this case, the size of the "zone of influence" seems to remain largely constant, but the level of predicted PEEQ increases with each load cycle. The modelling of high numbers of cycles leads eventually to unrealistically high PEEQ levels, indicating that failure mechanics or corrosion modelling could be introduced into the model. Techniques for modelling damage such as damage constitutive equations [46] or modelling crack propagation using XFEM [47, 48] could also be employed in anticipated future work.

The current capability in mathematical analysis to bound the stress-strain prediction error arising from surface roughness is still at a preliminary level, and there is significant work needed before this can become a robust tool for engineers.

The computational methods described here are feasible and robust, but the effort required to generate a suitable mesh means that further development work is required, to align the methods better for industrial application.

References

[1] Ed Leach, R. *Characterisation of areal surface texture*, Springer-verlang, Berlin Heidelbert, 2013.

[2] Wiśniewska, M. "The ISO 25178 standards for areal surface texture measurements: a critical appraisal," in *The challenges of contemporary science. Theory and applications*, Fundacja na Rzecz Młodych Naukowców, Warsaw, Poland, 97–98, 2014.

[3] Department of Defense Joint Service Specification Guide, Aircraft Structures, JSSG-2006, October 1998.

[4] EASA Certification Specifications and Acceptable Means of Compliance for Engines, CS-E, Amendment 4, 12 March 2015; sections AMC E 515 "Engine Critical Parts" and AMC E 650 "Vibration Surveys".

[5] Saint-Venant, A.J.C.B., "Memoire sur la Torsion des Prismes," *Mem. Divers. Savants*, **14**, 233–560, 1855.

[6] Love, A.E.H., *A Treatise on the Mathematical Theory of Elasticity*, 4th Ed., Cambridge University Press, 1944.

[7] Ainsworth, M. and Oden, J.T. *A Priori Error Estimation in Finite Element Analysis*, Wiley Interscience, New York, 2000.

[8] Armstrong, C.G.; McKeag, R.M.; Ou, H. and Price, M.A. "Geometric Processing for Analysis," Geometric Modeling and Processing 200: Theory and Applications Proceedings, February 2000.

[9] Robinson, T.; Armstong, C.G. and Chua, H.S., "Strategies for Adding Features to CAD Models in order to Optimize Performance," *Structural and Multidisciplinary Optimisation*, **46**(3), 2012.

[10] Hill, R. *The Mathematical Theory of Plasticity*, Oxford University Press, 1998.

[11] Jones R., Molent L., Barter S., Matthews N. and Tamboli D. "Supersonic particle deposition as a means for enhancing the structural integrity of aircraft structures," *Int. Journal of Fatigue*, **68**, pp. 260–268, 2014.

[12] Bowden, F.P. and Tabor, D., *The Friction and Lubrication of Solids*, Oxford University Press, 1964.

[13] Yu, G.; Li, H. and Walker, D. "Removal of Mid Spatial-Frequency Features in Mirror Segments," J. European Optical Society – Rapid Publications, vol. 6, pp. 11044, 2011.

[14] Curtis, S.; de los Rios, E.R.; Rodopulos, C.A. and Levers, A. "Analysis of the effects of controlled shot peening on fatigue damage of high strength aluminium alloys," *Int J Fatigue*, **25**, 59–66, 2003.

[15] Mandelbrot, B.B., "The Fractal Geometry of Nature," W.H. Freeman and Co, New York, 1982.

[16] Carpinteri, A. and Spagnoli A. "A fractal analysis of size effect on fatigue crack growth," *Int J Fatigue*; **26**, 125–33, 2004.

[17] Spagnoli, A. "Self-similarity and fractals in the Paris range of fatigue crack growth," *Mechanics of Materials*, **37**, 519–529, 2005.

[18] Jones R., Chen F., Pitt S., Paggi M. and Carpinteri A. "From NASGRO to fractals: Representing crack growth in metals," *Int J Fatigue*, **82**, 540–549, 2016.

[19] Molent L. and Jones R. "A Stress versus crack growth rate investigation (aka stress − cubed rule)," *Int J Fatigue*, **87**, 435–443, 2016.

[20] http://www.iso.org/iso/home.html [last accessed 2017/02/27].

[21] de Berg, M., Cheong, O.; van Kreveld, M. and Overmars, M. *Computational Geometry: Algorithms and Applications*, 3rd Ed., Springer, Berlin Heidelberg, 2008.

[22] Bakhvalov, N.S. and Panasenko, G.P. *Averging processes in periodic media*, Kluwer Aacdemic Publ., Dordrecht, 1989.

[23] Bensoussan, A. Lions, J.-L. and Papanicolau, G. *Asymptotic analysis for periodic structures, North-Holland*, Amsterdam, 1978.

[24] Chechkin, G.A.; Piatnitkski, A.L. and Shamaev, A.E. *Homogenization. Methods and applications*, Am. Math. Soc., Providence, RI, 2007.

[25] Jikov, V.V.; Kozlov, S.M. and Oleinik, O.A. *Homogenization of differential operators and integral functionals*, Springer-Verlang, Berlin etc., 1994.

[26] Marchenko, V.A. and Khruslov, E.Ya. *Homogenization of partical differential equations*, Birkhäuser, Boston, MA, 2006.

[27] Sánchez-Palencia, E. *Homogenization techniques for composite media*, Springer-Verlag, Berlin etc., 1987.

[28] Belyaev, A.G.; Piatnitski, A.L. and Chechkin, G.A. "Asymptotic behaviour of a solution to a boundary value problem in a perforacted domain with oscillating boundary," *Siberian Mathematical Journal*, **39**(4), 621–644, 1998 (translated in English from *Sibirskii Matematicheskii Zhurnal*, **39**(4), 730–754, 1998.

[29] Chechkin, G.A.; Friedman, A. and Piatnitkski, A.L. "The boundary value problem in domains with very rapidly oscillating boundary," *Journal of Mathematical Analysis and Applications (JMAA)*, **231**(1), 213–234, 1999.

[30] Amirat, Y.; Bodart, O.; Chechkin, G.A. and Piatnitski, A.L. "Boundary homogenization in domains with randomly oscillating boundary," *Stochastic Processes and their Applications*, **121**(1), 1–23, 2011.

[31] Chechkin, G. A.; Chechkina, T.P.; D'Apice, C.; De Maio, U. and Mel'nyk, T.A. "Asymptotic analysis of a boundary value problem in a cascade thick junction with a random transmission zone," *Applicable Analysis*, **88**(10–11), 1543-1562, 2009.

[32] Chechkin, G. A.; Chechkina, T.P.; D'Apice, C.; De Maio, U. and Mel'nyk, T.A. "Homogenization of a 3D thick cascade junction with the random transmission zone periodic in one direction," *Russ. J. Math. Phys.*, **17**(1), 35–55, 2010.

[33] Chechkin, G.A.; D'Apice, C.; De Maio, U.and Piatnitkski, A.L. "On the rate of convergence of solutions in domain with random multilevel oscillating boundary," *Asymptotic Analysis*, **87**(1–2), 1–28, 2014.

[34] ASTM (1998), Standard Practice for Conducting Force Controlled Constant Amplitude Axial Fatigue Tests of Metallic Materials, ASTM E646, USA.

[35] Lai, J.; Huang, H. and Buising, W. "Effects of microstructure and surface roughness on the fatigue strength of high-strength steels," *Procedia Structural Integrity*, **2**, 1213–1220, 2016. (21st European Conf. Fracture, EXF21, 20-24 June 2016, Catania, Italy.)

[36] Yuri, T.; Ono, Y. and Ogata, T. "Effects of surface roughness and notch on fatigue properties for Ti-5Al-2.5Sn ELI alloy at cryogenic temperatures," *Science and Technology of Advanced Materials*, **4**, 291–299, 2003.

[37] Abaqus manuals, Dassault Systèmes Simulia Corp., Providence, RI, USA.

[38] Brinckmann, S. and Van der Giessen, E. "A fatigue crack initiation model incorporating discrete dislocation plasticity and surface roughness," *Int J Fract*, **148**, 155–167, 2007.

[39] Vrac, D.; Sidjanin, L. and Balos, S. "The effect of honing speed and grain size on surface roughness and material removal rate during honing," *Acta Polytechnica Hungarica*, **11**(10), 163–175, 2014.

[40] Ali, K.; Peng, D.; Jones, R.; Singh, R.R.K.; Zhao, X. L.; McMillan, A.J. and Berto, F. "Crack growth in a naturally corroded bridge steel," *Fatigue and Fracture of Engineering Materials and Structures*, 2016, doi: 10.1111/ffe.12568.

[41] Jones, R. "Fatigue Crack Growth and Damage Tolerance", Invited Review Paper, *Fatigue and Fracture of Engineering Materials and Structures*, **37**(5), 463–483, 2014.

[42] Jones, R.; Huang, P. and Peng, D. "Crack growth from naturally occurring material

discontinuities under constant amplitude and operational loads," *Int J Fatigue*, **91,** 434–444, 2016.

[43]   Molent, L.; Jones, R. "The influence of cyclic stress intensity threshold on fatigue life scatter," *Int J Fatigue*, **82,** 748–756, 2016.

[44]   Berens, A.P.; Hovey, P.W. and Skinn, D.A. *Risk analysis for aging aircraft fleets - Volume 1: Analysis,* WL-TR-91-3066, Flight Dynamics Directorate, Wright Laboratory, Air Force Systems Command, Wright-Patterson Air Force Base, October 1991.

[45]   Molent, L.; Barter, S.A. and Wanhill, R.J.H. "The lead crack fatigue lifing framework," *Int J Fatigue*, **33,** 323–331, 2011.

[46]   Lemaitre, J. "Coupled elasto-plasticity and damage constitutive equations," *Computer Methods in Apllied Mechanics and Engineering*, **51**, 31–49, 1985.

[47]   Ed Leach, R. *Characterisation of areal surface texture*, Springer-verlang, Berlin Heidelbert, 2013.

[48]   Wiśniewska, M. "The ISO 25178 standards for areal surface texture measurements: a critical appraisal," in *The challenges of conteporary science. Theory and applications*, Fundacja na Rzecz Młodych Naukowców, Warsaw, Poland, 97–98, 2014.